FILTER SYNTHESIS

AN OVERVIEW OF CLASSICAL FILTERS

Electrical filters are, as a rule, lossless two-ports embedded in resistances R_1 and R_2, as shown in Fig. 1. A lossless two-port may only contain inductors, capacitors, and ideal transformers. The filters allow a band of the input frequencies to pass with only a small attenuation while all remaining fre-

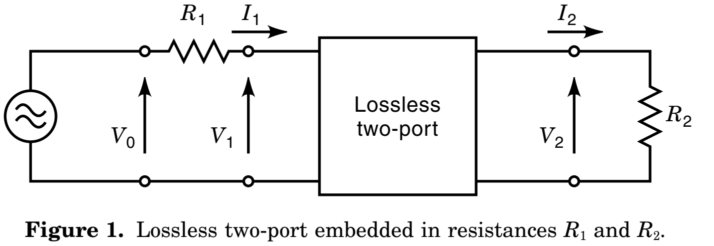

Figure 1. Lossless two-port embedded in resistances R_1 and R_2.

quencies are to a large extent suppressed. The transfer function

$$\frac{V_2(p)}{V_0(p)} = F^*(p) \tag{1}$$

also called the transfer voltage ratio or the insertion voltage gain, is a function of the complex frequency p, where $p = j\omega$ stands for the natural and measurable angular frequencies ω. For brevity ω will from now on be called simply the frequency. From $F^*(j\omega) = A(\omega)e^{j\varphi(\omega)}$ are derived the magnitude $A(\omega) = |F^*(j\omega)|$ and the phase $\varphi(\omega) = \arg F^*(j\omega)$ with the group delay $\tau(\omega) = -d\varphi(\omega)/d\omega$. The attenuation function is $a(\omega) = -20 \log|F^*(j\omega)|$ in dB (decibels) or, more seldom, $\ln|F(j\omega)|$ in Np (nepers). The relation is 1 Np = 8.686 dB.

The synthesis of filters follows a well-established pattern. First the properties of a transfer function $F^*(p)$ of a two-port with given types of components have to be established. This guarantees the existence of a solution with realizable positive values of the components as long as the desired transfer function exhibits the before-mentioned properties. The most common types of components for classical filters are lossless inductors and capacitors, as well as ideal transformers for the two-port and resistances R_1 and R_2 as internal resistance of the source and as the terminating load. This case is treated in this article. Other types of components are switches such as FETs, capacitors, and operational amplifiers in so-called switched capacitor filters or delays, adders and multipliers in digital filters or resistors, capacitors and operational amplifiers in RC-active filters, or electro-mechanical transducers and a set of electrodes in surface acoustic wave (SAW) filters which are treated in the last section.

The next step in filter synthesis is the approximation of given specifications for a particular filter by functions meeting the requirements of $F^*(p)$. The last step is the calculation of the values of the components by mathematical means from the functions approximating the specifications. This step also provides the topology of the two-port. For approximations it is mathematically easier to handle the square of the magnitude $|F^*(j\omega)|^2$. For a lossless two-port in Fig. 1 $F^*(p)$ has the following properties (1,2):

1. $F^*(p)$ is a rational function in p, real valued for real-valued p; as a consequence, the coefficients in $F^*(p)$ are real valued if the numerator and the denominator of $F^*(p)$ do not contain a common complex factor.
2. Stability requires the poles of $F^*(p)$ to lie in Re $p < 0$ and the degree of the numerator not to exceed the degree of the denominator. The denominator is hence a Hurwitz polynomial.
3. The numerator is either an even or an odd polynomial in p if common factors in the numerator and the denominator are not cancelled.
4. The maximum power available at the output reveals the upper bound (Feldtkeller condition).

$$|F^*(j\omega)| \le \frac{1}{2}\sqrt{\frac{R_2}{R_1}} = \frac{1}{q} \tag{2}$$

A given $F^*(p)$ meeting these requirements is always realizable by a lossless two-port embedded in R_1 and R_2. $|F^*(j\omega)|^2$ can also be expressed by the reflection coefficient introduced by S. Darlington (3)

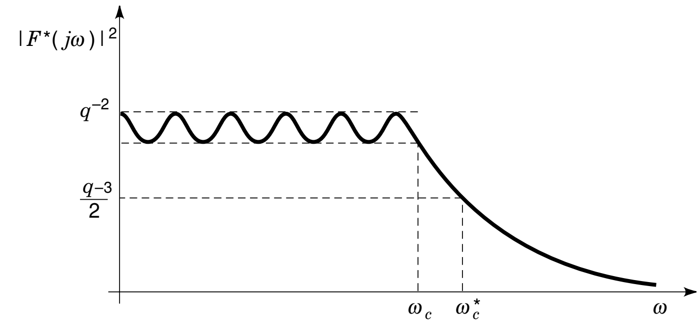

Figure 2. Low-pass with cutoff frequency ω_c, 3 dB cutoff frequency ω_c^*, and the equiripple between q^{-2} and $q^{-2} - a^2$.

$$S_{11}(j\omega) = \frac{R_1 - Z_1(j\omega)}{R_1 + Z_1(j\omega)} \tag{3}$$

as

$$|F^*(j\omega)|^2 = \frac{R_2}{4R_1}(1 - |S_{11}(j\omega)|^2) \tag{4}$$

where $Z_1(j\omega)$ represents the input impedance of the two-port loaded by R_2. S_{11} is an element of the scattering matrix. Instead of transfer functions the inverse of the transfer function V_0/V_2 or $V_0/2V_2$ is also applied. These functions are also called the insertion voltage loss. In this article

$$\frac{V_0(p)}{V_2(p)} = K^*(p) \tag{5}$$

will be used.

The insertion loss (4),

$$20 \log \frac{R_2}{R_1 + R_2} \left| \frac{V_0(j\omega)}{V_2(j\omega)} \right| = 10 \log \frac{P_0}{P_2} \tag{6}$$

is based on the ratio between the power $P_0 = |V_0(j\omega)|^2 R_2/(R_1 + R_2)^2$ dissipated in R_2 without the two-port inserted in between the source V_0 with R_1 and the load R_2 and the power $P_2 = |V_2(j\omega)|^2/R_2$ dissipated in R_2 in the presence of the two-port.

Figures 2 through 5 depict examples for $|F^*(j\omega)|^2$ of characteristic filters, such as a low-pass, a high-pass, a bandpass,

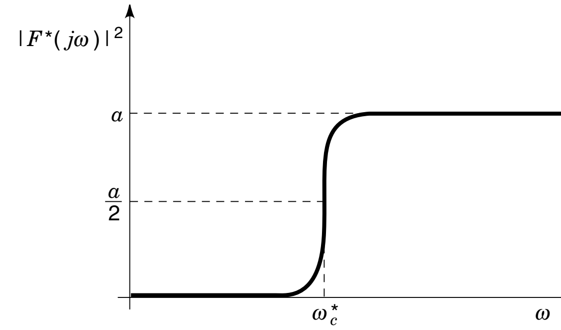

Figure 3. High-pass filter.

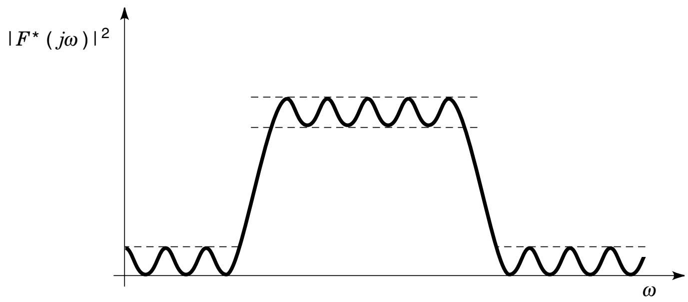

Figure 4. Bandpass filter.

and a bandstop. The beginning and the end of the passband are defined by a cutoff frequency ω_c or ω_c^*. For the low-pass in Fig. 2, ω_c^* is chosen as the frequency, where $|F^*(j\omega)|^2$ has decreased to 1/2 of the value at $\omega = 0$ (3 dB frequency).

Another choice is a specific frequency ω_c. For example, in Fig. 2 $|F^*(j\omega)|^2$ leaves the band of equiripple behavior, later also called Chebyshev behavior.

A typical example for a low-pass circuit is shown in Fig. 6. The zeros of $F^*(p)$ that generate a zero output voltage are visible in the circuit diagram. The series parallel resonator exhibits an infinite impedance at the resonant frequency ω_1, preventing signals from reaching the output. The same is true for the shunt series resonator exhibiting a zero impedance at the resonant frequency ω_2. Finally, a zero output is observed at $\omega = \infty$ because the shunt capacitors have a zero impedance and the series inductor exhibits an infinite impedance. Nonideal resonators represent a resistor R at the resonant frequency. The larger the quality factor Q of a resonator is, the better the transmission zero is realized. For series resonators $Q = Z/R$, whereas for parallel resonators $Q = R/Z$ with $Z = \sqrt{L/C}$. L stands for the value of the inductor and C for the value of the capacitor. $|F^*(j\omega)| =$ const. means a lack of amplitude distortion; together with an arbitrary phase $\varphi(\omega)$ it defines an allpass, the transfer function of which is

$$F^*(p) = k\frac{r(-p)}{r(p)}$$

where $r(p)$ is a Hurwitz polynomial in p and k a constant. $F^*(p)$ with a linear phase $\varphi(\omega) = -\omega t_0$ reflecting in a constant group delay t_0 and with an arbitrary magnitude belongs to a two-port without phase distortion. $F^*(p)$ with a constant nonzero magnitude in $|\omega| \in [0, \omega_C]$, zero magnitude otherwise,

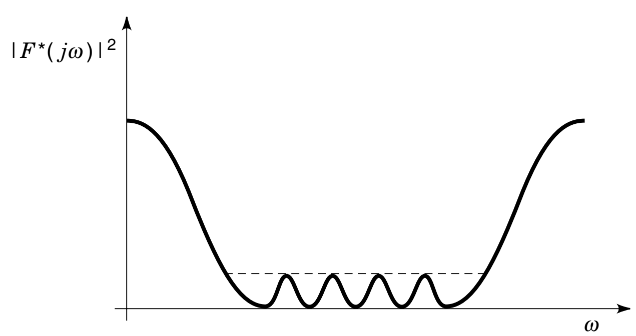

Figure 5. Bandstop filter.

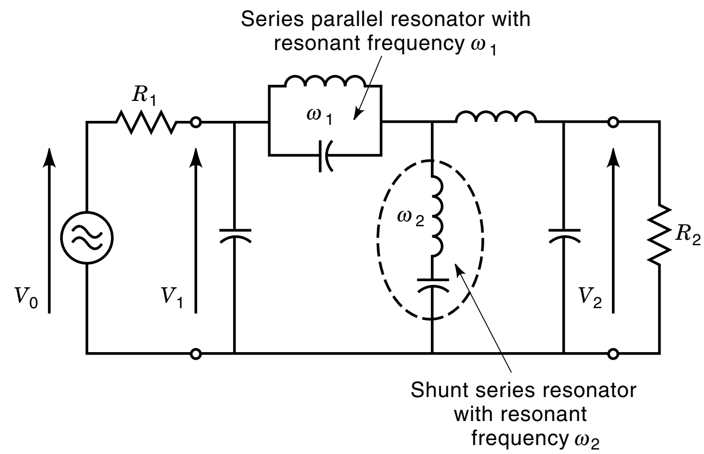

Figure 6. Example of a lowpass circuit.

and a linear phase $-\omega t_0$ is called an ideal low-pass, which works as a delay line with delay t_0 for frequencies in the passband.

A filter cascaded by an amplitude equalizer exhibits an overall transfer function with an approximately constant magnitude, whereas a phase equalizer in cascade provides a linear phase of the overall two-port (4). The phase equalizer is an allpass.

If all reactances in a two-port are discharged at time $t = 0$, then $F^*(p)$ is the Laplace transform of the impulse response $h(t)$ with

$$h(t) = \frac{1}{2\pi j}\int_{\sigma-j\infty}^{\sigma+j\infty} F^*(p)e^{pt}dp$$

where $F^*(p)$ is an analytical function in Re $p \geq \sigma_0 \leq \sigma$. The step response is

$$a(t) = \int_{0_-}^{t} h(\tau)d\tau$$

Some lowpasses with specific characteristics are discussed together with amplitude and phase equalizers in the following subsections.

Guidelines will be presented on how to determine from filter tables the component values of a filter meeting given specifications. This should enable a system engineer to achieve a quick filter design by selecting the appropriate type of filter and by then finding the component values in a table.

Butterworth Low-passes

A Butterworth lowpass (9) in Fig. 7 exhibits a maximum flat magnitude $|F^*(j\omega)|$ at $\omega = 0$—that is, $d^\nu\,|F^*(j\omega)|/d\omega^\nu = 0$ for $\nu = 1, 2, \cdots n$, where n is the degree of $F^*(p)$. The decay of the magnitude is moderately steep in the transition region and approaches $n \times 20$ dB per frequency decade for large values of ω. $K^*(p) = 1/F^*(p)$ is a polynomial.

We investigate the step response $a(t)$ for various lowpasses, including the Butterworth low-pass. To compare $a(t)$ for those lowpasses, we normalize all of them with the frequency ω_c, where $|F^*(j\omega_c)| = 0.9 \times F^*(0)$ holds. For low-passes with equiripple behavior, ω_c also stands for the end of the

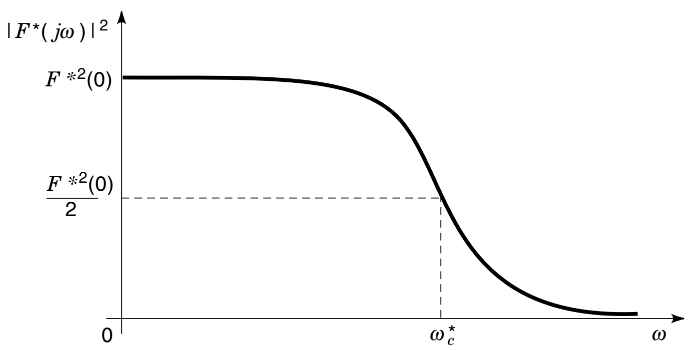

Figure 7. A Butterworth low-pass, maximally flat at $\omega = 0$.

Table 1(a). Overshoot and Rise Time of Butterworth Low-passes with $F^*(p)$ of Degree $n = 1$ to 7.

n	Overshoot, In %	Rise Time, 10 To 90%, In τ
1	0	1.06
2	4.32	1.50
3	8.15	1.80
4	10.83	2.03
5	12.78	2.22
6	14.25	2.38
7	15.41	2.51

Normalizing frequency ω_c is given by $|F^*(i\omega_c)| = 0.9 \times F^*(0)$ leading to the normalized time $\tau = \omega_c t$.

equiripple band. The normalized time is $\tau = \omega_c t$. Figure 8 shows $a(\tau)/a(\infty)$ for a Butterworth low-pass with $F^*(p)$ of seventh degree (10). There is an overshoot of 15.4% over the value $a(\infty)$, the largest of the low-passes compared, but followed by rapidly decreasing oscillations around the value $a(\infty)$. Values for the overshoot in % and for the rise time in τ from 10 to 90% of $a(\infty)$ are listed in Table 1(a) for Butterworth low-passes with $F^*(p)$ of degree 1 to 7. For a Butterworth low-pass with $F^*(p)$ of 7th degree the rise time is $t = 2.51\omega_c^{-1}$, the 2nd smallest rise time of all low-passes in Table 1(e).

Thomson Low-passes

Thomson low-passes (11) are given by $K^*(p) = 1/F^*(p)$ representing a modified Bessel polynomial. They are therefore often also called Bessel low-passes. $F^*(p)$ exhibits a maximum flat group delay t_0 at $\omega = 0$. The decay of the magnitude is moderately steep in the transition region and for a large ω is again $n \times 20$ dB/decade, where n is the degree of $F^*(p)$. The step response $a(\tau)/a(\infty)$ for the Thomson low-pass with $n = 7$ is plotted in Fig. 8 (10). It is a remarkably good approximation of an undistorted delayed step. The overshoot is only 0.49% over $a(\infty)$. Oscillations around $a(\infty)$ are only marginal.

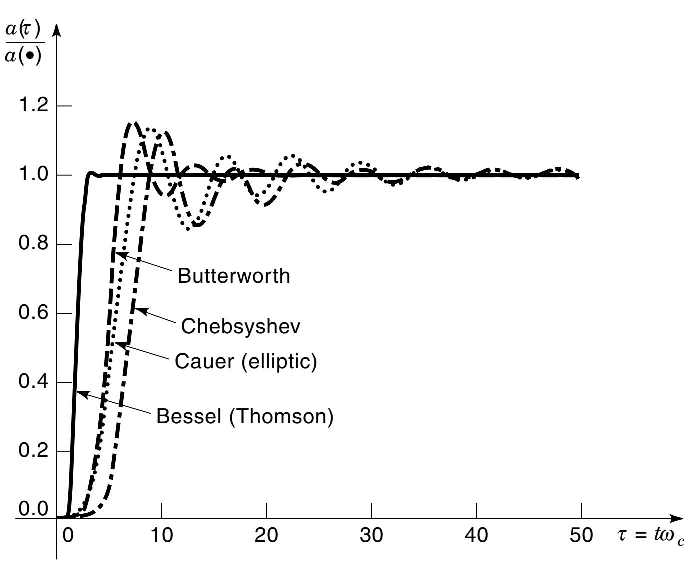

Figure 8. Step responses $a(\tau)/a(\infty)$ of various filters with transfer functions $F^*(p)$ of seventh degree. The common characteristics of the filters are provided in the caption and footnote of Table 1(a).

Table 1(b) contains values for overshoot and rise time of $a(\tau)$ for $n = 1$ to 7 (10). The rise time for $n = 7$ is according to Table 1(e) $t = 1.22\omega_c^{-1}$, the smallest value of all low-passes listed in Table 1(e).

Chebyshev Low-passes

Chebyshev low-passes (Fig. 2) possess a magnitude oscillating between two constant boundaries in the passband, where each extremum touches the boundaries. This is called an equiripple, or a Chebyshev behavior in the passband. $K^*(p) = 1/F^*(p)$ is a polynomial. The larger the ripple a^2 in Fig. 2 the steeper is the decay of $|F^*(j\omega)|^2$ in the transition region from the passband into the stopband. From all polynomials this decay is steepest. However, independent of a^2 the decay at large ωs is again $n \times 20$ dB/decade. The step response $a(\tau)/a(\infty)$ for $n = 7$ in Fig. 8 (10) exhibits the third largest overshoot over $a(\infty)$; however, the oscillations around $a(\infty)$ decay rather rapidly. According to Table 1(e) the value for the overshoot is 12.7%, whereas the rise time is $t = 3.4\omega_c^{-1}$, the 2nd largest value in Table 1(e). Overshoot and rise time of $a(\tau)$ for $n = 1$ to 7 are listed in Table 1(c) (10).

Cauer Filters as Low-passes

Elliptic filters or Cauer filters (12) (Fig. 9) are low-passes exhibiting an equiripple behavior both in the passband and in the stopband. They arebased on elliptic integrals which is why they are also called elliptic filters. $K^*(p) = 1/F^*(p)$ is a rational function in p. The step response of the Cauer low-passes for $n = 7$ in Fig. 8 exhibits the second largest overshoot and only slowly decaying oscillations around $a(\infty)$ (10). Overshoot and rise time for $n = 1$ to 7 are listed in Table

Table 1(b). Overshoot and Rise Time of Thomson Low-passes with $F^*(p)$ of Degree $n = 1$ to 7.

n	Overshoot, In %	Rise Time, 10 To 90%, In τ
1	0	1.06
2	0.43	1.21
3	0.75	1.25
4	0.84	1.25
5	0.77	1.24
6	0.64	1.23
7	0.49	1.22

Normalization as in Table 1(a).

Table 1(c). Overshoot and Rise Time of Chebyshev Low-passes with $F^*(p)$ of Degree $n = 1$ to 7.

n	Overshoot, in %	Rise Time, 10 to 90%, in τ
1	0	1.06
2	14.0	1.59
3	6.82	2.36
4	21.2	2.45
5	10.7	2.98
6	24.25	2.95
7	12.68	3.40

Normalization as in Table 1(a).

Table 1(d). Overshoot and Rise Time of Cauer Low-passes with $F^*(p)$ of Degree $n = 1$ to 7.

n	Overshoot, in %	Rise Time, 10 to 90%, in τ
1	0	1.06
2	14.0	1.59
3	7.10	2.38
4	22.2	2.57
5	12.2	3.23
6	25.9	3.31
7	13.72	3.81

Normalization as in Table 1(a); in addition, minimum attenuation in stopband 60 dB.

1(d) (10). In addition to the properties of the normalization mentioned previously for Butterworth low-passes, the minimum stopband attenuation of the Cauer filters is chosen to be 60 dB.

Table 1(e) shows a comparison of overshoot and rise time of the step response for four filter types with $F^*(p)$ of degree 7.

Further filters such as bandpasses, high-passes, bandstops, or filters with several passbands are obtained by a frequency transformation applied to the low-pass, where the frequency characteristics are preserved.

Design of Filters by Using Filter Tables

There are three characteristic low-passes tabulated to choose from for a given task. They are the Butterworth, the Chebyshev, and the Cauer low-pass, the features of which have been discussed above. The Bessel low-pass is, as a rule, not contained in tables as it main deals with properties in the time domain.

After the selection of the appropriate type of low-pass the designer turns to the pertinent filter tables. As a rule only solutions for the special case $R_1 = R_2$ are tabulated. If this is not acceptable because an additional amplifier may be required one has to go through the general design procedure as described in the next paragraph. The general procedure is also mandatory if different types of specifications are given, such as steps in the attenuation in the stopband or the suppression of specific pilot frequencies.

As shown in Fig. 12, the filter requirements are given by four values for the attenuation $a(\Omega) = -20 \log|F^*(j\Omega)|$ in dB, where

$$\Omega = \frac{\omega}{\omega_c} \tag{7a}$$

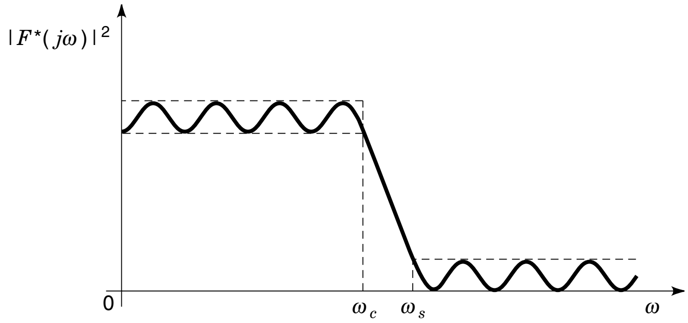

Figure 9. A Cauer low-pass (elliptic filter) with equiripple in passband and stopband; ω_s is end of transition region.

is the normalized frequency. Those four values in dB are A_0 the minimum attenuation in the passband, $A_{\max}$ the maximum attenuation in the passband, $A_{\min}$ the minimum attenuation in the stopband, and the frequency Ω_s defining the end of the transition region with $a(\Omega_s) = A_{\min}$. For $R_1 = R_2$ we obtain $A_0 = 0$ as a special case. This reduces the number of specifications to three.

First the reflection coefficient $\rho = \sqrt{1 - 10^{-0.1A_{\max}}}$ has to be calculated. A table with $A_{\min} + 10\log(\rho^{-2} - 1)$ as ordinate and Ω_s as abcissa reveals the required degree n for a given Ω_s, ρ, $A_{\min}$, and filter type. Then one turns to tables for the chosen type of low-pass, the degree n and the value ρ which provide the normalized values of the components.

The normalized values ℓ and c of the reactances provided by the tables are with a normalizing resistor R_1

$$\frac{\omega L}{R_1} = \frac{\omega}{\omega_c}\frac{\omega_c L}{R_1} = \Omega \times \ell \tag{7b}$$

and

$$\omega C R_1 = \frac{\omega}{\omega_c}\omega_c C R_1 = \Omega \times c \tag{7c}$$

where

$$\ell = \frac{\omega_c L}{R_1} \tag{8a}$$

and

$$c = \omega_c C R_1 \tag{8b}$$

ℓ and c are values without dimension.

Table 1(e). Comparison of Overshoot and Rise Time of the Step Response for Four Low-passes with $F^*(p)$ of Degree 7.

Low-Pass Type	Overshoot, in %	Rise Time, 10 to 90%, in τ
Thomson	0.49	1.22
Butterworth	15.4	2.51
Chebyshev	12.7	3.40
Cauer	13.7	3.81

Normalization as in Table 1(a).

The denormalized values are, for the inductors

$$L = \frac{R_1}{\omega_c} \cdot l$$

and for the capacitors

$$C = \frac{1}{\omega_c R_1} \cdot c$$

This conclude the design with the help of a table.

Equalization of Amplitude and Phase

In systems the need can arise to change the amplitude, that is the attenuation $a(\omega)$, most often to render it constant in a given range of frequencies. A simple solution is to replace the resistance R_2 at the output by a two-port with input resistance $R = R_2$, but a frequency-dependent inverse transfer function $K_B^*(p)$ and the associated attenuation $a(\omega) = 10 \log|K_B^*(j\omega)|^2$. $K_B^*(p)$ is multiplied with the inverse transfer function of the given two-port, whereas $a(\omega)$ is added to its attenuation. Such an amplitude equalizer is shown in Fig. 38 with the design equation in the figure caption. If several of those equalizers have to be cascaded it is easily done by replacing the loading resistance $R = R_2$ of the first equalizer by the next equalizer and so on. Table 5 shows $a(\omega)$ for various equalizer two-ports. The shapes of $a(\omega)$ are chosen such that they add to the attenuation to be equalized at the frequencies where this is needed. The equalizers however also change the phase of the entire two-port which is tolerable for all filters where phase is not important, such as in audio systems.

The correction of the phase or the group delay of a given two-port is done by cascading phase equalizers at the output of the given two-port. They are allpasses as depicted in Fig. 40. The phase equalizers exhibit an input resistance $R = R_2$ if terminated by R_2 thus replacing the load R_2 of the given two-port. The design equations are given in the caption of Fig. 40. The equalizers further offer a unit magnitude that is an attenuation $a(\omega) = 0$ and a group delay as shown in Figs. 39(a) and 39(b). By cascading two-ports the transfer functions are multiplied and hence the phases in the exponent of the exponential functions are added. This also applies to the group delay. The attenuation of the given two-port remains unchanged due to $a(\omega) = 0$ of the allpasses. Figs. 39(a) and 39(b) reveal how the allpasses must be chosen to add to the group delay at those frequencies where an increase is needed. Most often the group delay has to become constant by a phase equalization.

So far we have dealt with two-ports. There are also m-n-ports with n input ports and m output ports. They can realize filter banks.

THE SYNTHESIS OF FILTERS

To obtain general results for low-passes independent of the values of the cutoff frequencies ω_c, we introduce a normalized frequency $\Omega = \omega/\omega_c$ pertaining to the s-plane with the imaginary axis $s = j\Omega$. This translates $K^*(p)$ in Eq. (5) in which $p = j\omega$ as follows:

$$\frac{V_0}{V_2} = K^*(j\omega) = K^*\left(j\frac{\omega}{\omega_c}\omega_c\right) = K^*(j\Omega\omega_c) = K(j\Omega)$$

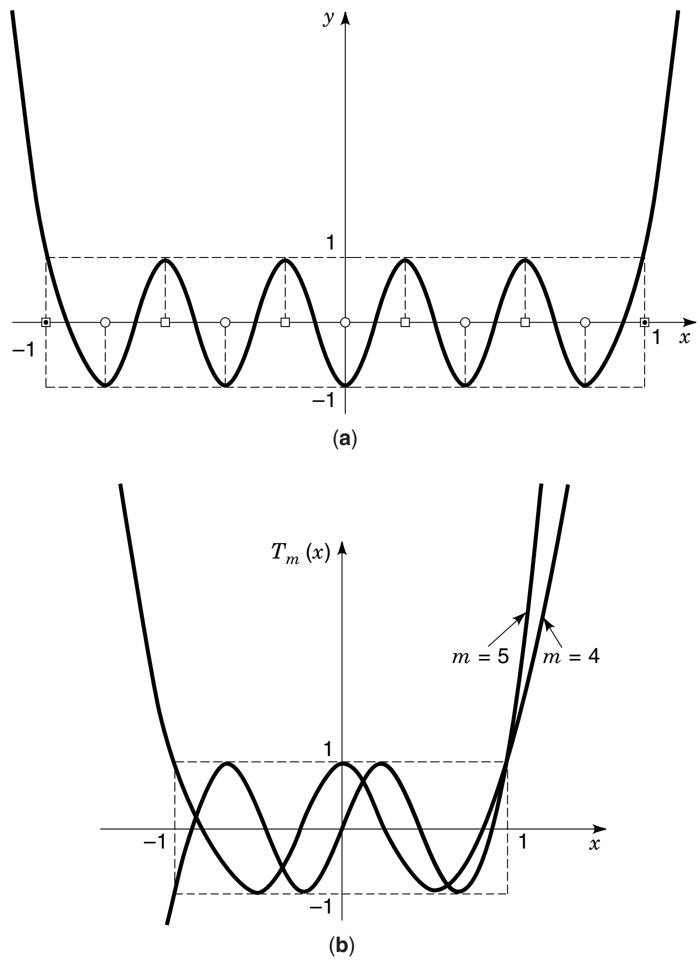

Figure 10. (a) A Chebyshev polynomial $y(x)$. (b) The Chebyshev polynomial of fourth and fifth degree m.

and hence

$$\frac{V_0}{V_2} = K^*(p) = K(s)$$

The synthesis follows the steps as listed and explained here:

1. The given tolerance scheme for $|K(j\Omega)|^2 = P(\Omega)$ is approximated by a realizable

$$|K(j\Omega)|^2 \geq q^2 = 4\frac{R_1}{R_2} \tag{9}$$

with q in Eq. (2).

2. From $|K(j\Omega)|^2$ the function $K(s)$, the characteristic function $f(s)$; and the elements of the chain matrix $A(s)$ are determined.
3. $A(s)$ is realized by a lossless two-port by a pole removal process.

Calculations For The Individual Steps

The approximation and calculation may be performed by a general approach based on a least square procedure. However, as a rule, special functions with suitable properties are chosen to solve the approximation problem. These functions

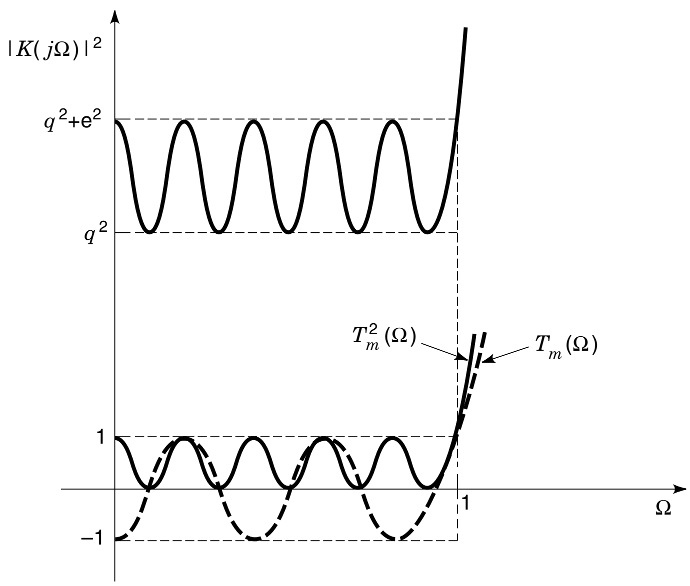

Figure 11. The square of the magnitude $|K(j\Omega)|^2$ of a Chebyshev low-pass with $|K(j\Omega)|^2 = e^2T_m^2(\Omega) + q^2$.

will be discussed. Finally, a general approximation procedure based on a conformal mapping will be outlined.

The Chebyshev Approximation and the Calculation of *K*(*s*). The square $|K(j\Omega)|^2$ of the magnitude of the function $K(j\Omega)$ according to the Chebyshev approximation is plotted in Fig. 11. In the passband $|K(j\Omega)|^2$ completely exhausts the tolerance stripe; that is, each extremum of $|K(j\Omega)|^2$ touches the limit of the tolerance band from the inside. In the stopband $|K(j\Omega)|^2$ tends to infinity. As these filter characteristics are most widely used, more detailed information on the Chebyshev approximation must be given. The differential equation for a Chebyshev polynomial $y(x)$ is

$$m^2(1-y^2) = \left(\frac{dy}{dx}\right)^2(1-x^2) \tag{10a}$$

or

$$m^2(y^2-1) = \left(\frac{dy}{dx}\right)^2(x^2-1) \tag{10b}$$

where m is a constant. The differential equation equates the zeros in Fig. 10(a) of $y + 1$ ○ and $y - 1$ □ with the zeros of y'^2 and $x - 1$ ● as well as $x + 1$ ●. The statement

$$x = \cos\vartheta \text{ and } y = \cos\eta$$

provides the solution

$$y = \cos(m\vartheta + c) \text{ with } \vartheta = \arccos x \text{ for } |x| \le 1$$

whereas the statement

$$x = \cosh\vartheta \text{ and } y = \cosh\eta$$

yields the solution

$$y = \cosh(m\vartheta + c) \text{ with } \vartheta = \operatorname{arcosh} x \text{ for } |x| \ge 1$$

where c is the integration constant. For $c = 0$ we obtain

$$T_m(x) = y = \cos m\vartheta \tag{11a}$$

and

$$\vartheta = \arccos x \text{ for } |x| \le 1 \tag{11b}$$

and

$$T_m(x) = y = \cosh m\vartheta \tag{12a}$$

and

$$\vartheta = \operatorname{arcosh} x \text{ for } |x| \ge 1 \tag{12b}$$

The known trigonometric equality

$$\cos(m+1)\vartheta = \cos m\vartheta\cos\vartheta - \sin m\vartheta\sin\vartheta = \cos m\vartheta\cos\vartheta - \frac{1}{2}(\cos(m-1)\vartheta - \cos(m+1)\vartheta)$$

yields

$$\cos(m+1)\vartheta = 2\cos m\vartheta\cos\vartheta - \cos(m-1)\vartheta$$

or the recursion for $T_{m+1}(x)$:

$$T_{m+1}(x) = 2T_m(x)\times x - T_{m-1}(x) \tag{13}$$

The starting solutions for $m = 0$ and $m = 1$ are provided by Eqs. (11a) and (11b) as $T_0(x) = 1$ and $T_1(x) = x$. Some polynomials $T_m(x)$ for $m = 2, 3, \ldots 11$ obtained from Eq. (13) are listed in Table 2 and plotted for $m = 4$ and $m = 5$ in Fig. 10(b). Even m provide even and odd m odd polynomials $T_m(x)$. The coefficient at the leading term x^m is 2^{m-1}.

We first construct the function $V_0/V_2 = K(s)$ from a given $|K(j\Omega)|^2$. $|K(j\Omega)|^2 = P(\Omega)$ in Fig. 11 is expressed by

$$|K(j\Omega)|^2 = \epsilon^2T_m^2(\Omega) + q^2 = P(\Omega) \tag{14}$$

For $\Omega \gg 1$ we obtain with the coefficient 2^{m-1} of the leading term

$$|K(j\Omega)|^2 \approx \epsilon^2 2^{2(m-1)}\Omega^{2m} \tag{15}$$

and

$$a(\omega) = 10\log|K(j\Omega)|^2 \approx 20[m\log\Omega + (m-1)\log 2 + \log\epsilon] \tag{16}$$

Table 2. Chebyshev Polynomials of Degree 2 to 11.

$T_2(x) = 2x^2 - 1$
$T_3(x) = 4x^3 - 3x$
$T_4(x) = 8x^4 - 8x^2 + 1$
$T_5(x) = 16x^5 - 20x^3 + 5x$
$T_6(x) = 32x^6 - 48x^4 + 18x^2 - 1$
$T_7(x) = 64x^7 - 112x^5 + 56x^3 - 7x$
$T_8(x) = 128x^8 - 256x^6 + 160x^4 - 32x^2 + 1$
$T_9(x) = 256x^9 - 576x^7 + 432x^5 - 120x^3 + 9x$
$T_{10}(x) = 512x^{10} - 1280x^8 + 1120x^6 - 400x^4 + 50x^2 - 1$
$T_{11}(x) = 1024x^{11} - 2816x^9 + 2816x^7 - 1232x^5 + 220x^3 - 11x$

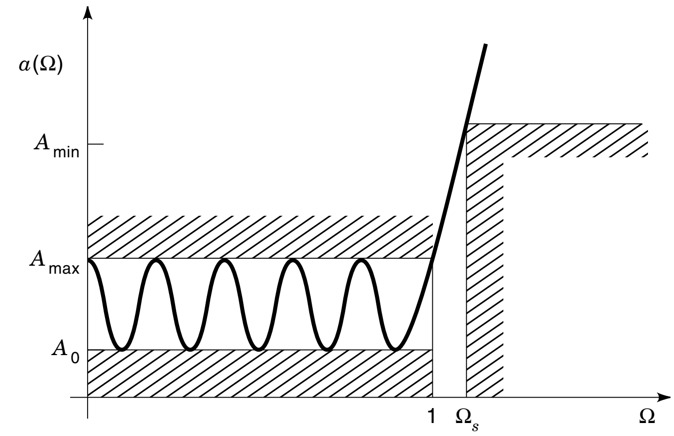

Figure 12. The tolerance scheme in decibels for a Chebyshev low-pass.

This reveals that for a small ripple $\epsilon < 1$, $\log \epsilon < 0$ decreases the rise of the attenuation for large Ω and for a large ripple $\epsilon > 1$, $\log \epsilon > 0$ increases the rise of the attenuation for large Ω. The increase of $a(\Omega)$ for a decade 10 Ω is $\Delta a(\Omega) = 20\ m$; that is, 20 dB per decade and per degree m of $T_m(\Omega)$. The attenuation $a(\omega)$ belonging to Fig. 11 is depicted in Fig. 12 with minimum (respectively maximum) attenuation A_0 (respectively, $A_{\max}$) in the passband and the minimum attenuation $A_{\min}$ in the stopband. The upper limit of the transition region is Ω_s. Chebyshev filters represent the rare case in which all characteristic values q, ϵ, and m in Eq. (14) can be determined from the given values A_0, $A_{\max}$, and $A_{\min}$ at Ω_s by the equations

$$10 \log q^2 = A_0$$

and hence

$$q^2 = 10^{A_0/10} \tag{17}$$

$$10 \log(q^2 + \epsilon^2) = A_{\max}$$

and hence

$$\epsilon^2 = 10^{A_{\max}/10} - 10^{A_0/10} \tag{18}$$

and

$$a(\Omega_s) = 10 \log(q^2 + \epsilon^2 \cosh^2 m \times \operatorname{arcosh} \Omega_s) = A_{\min}$$

and hence

$$m = \frac{1}{\operatorname{arcosh} \Omega_s} \operatorname{arcosh} \frac{\sqrt{10^{A_{\min}/10} - 10^{A_0/10}}}{\sqrt{10^{A_{\max}/10} - 10^{A_0/10}}} \tag{19}$$

In Eq. (19) the expression for $T_m(\Omega)$ for $|\Omega| \geq 1$ was used.

The general synthesis procedure outlined next was established by W. Bader (1,16a,16b). It is explained with Chebyshev low-passes as an example.

From the known $|K(j\Omega)|^2$ we have to calculate the rational function $K(s)$. We consider

$$|K(j\Omega)|^2 = P(\Omega) = P\left(\frac{s}{j}\right) = Q(s) \tag{20}$$

for $s = j\Omega$ and extend s into the entire complex plane. On the other hand, as $K(s)$ is real for real s, we obtain

$$|K(j\Omega)|^2 = K(j\Omega)\overline{K(j\Omega)} = K(j\Omega)K(-j\Omega) = K(s)K(-s) \tag{21}$$

for $s = j\Omega$, which is also extended into the s-plane. Equations (20) and (21) hence provide

$$K(s)K(-s) = Q(s) \tag{22a}$$

Obviously, $Q(s)$ is even in s, and real for real s. Hence the zeros occur at $s = s_i$ and $s = -s_i$ as well as at $s = \overline{s_i}$ and $s = -\overline{s_i}$, as plotted in Fig. 13. For $q = 0$, zeros on $s = j\Omega$ are feasible and have an even multiplicity. The zeros in Re $s < 0$ and half the multiplicity of the zeros on $s = j\Omega$ are assigned to $K(s)$, thus forming a stable or at least quasi-stable $K(s)$ if the zeros on $s = j\Omega$ are single. We perform these operations on $|K(j\Omega)|^2$ in Eq. (14) starting from $P(\Omega)$ and $Q(s)$ in Eqs. (20) and (22b), which yields

$$Q(s) = q^2 + \epsilon^2 T_m^2\left(\frac{s}{j}\right) = 0 \tag{22b}$$

or

$$T_m^2\left(\frac{s}{j}\right) = -\left(\frac{q}{\epsilon}\right)^2 \tag{23}$$

As the zeros are complex, we form

$$T_m\left(\frac{s}{j}\right) = \cos m\vartheta = \cos m(\vartheta_1 + j\vartheta_2) \quad \text{and} \quad \frac{s}{j} = \cos\vartheta \tag{24}$$

from which follows

$$T_m\left(\frac{s}{j}\right) = \cos m\vartheta_1 \cosh m\vartheta_2 - j \sin m\vartheta_1 \sinh m\vartheta_2 = \pm j\left(\frac{q}{\epsilon}\right) \tag{25}$$

The solutions are

$$\cos m\vartheta_1 \cosh m\vartheta_2 = 0$$
$$\sin m\vartheta_1 \sinh m\vartheta_2 = \mp\frac{q}{\epsilon}$$

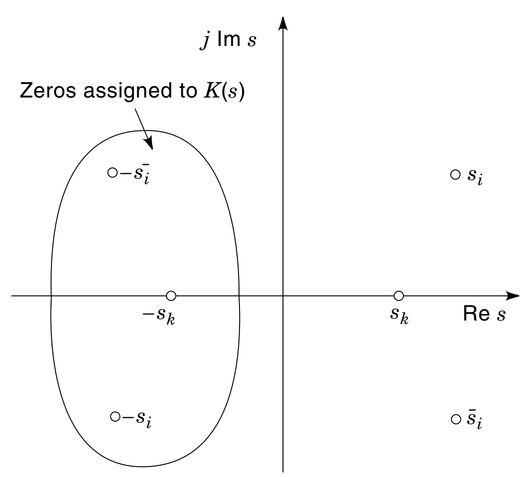

Figure 13. Zeros of $Q(s) = K(s)K(-s)$ in Eq. (22a).

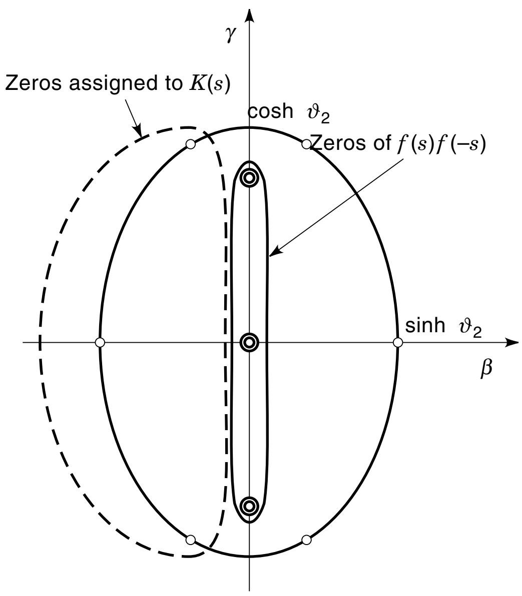

Figure 14. Zeros of $K(s)K(-s)$ and $f(s)f(-s)$ for Chebyshev filters with $m = 3$.

or

$$\vartheta_1 = \frac{2\nu + 1}{m}\frac{\pi}{2} \qquad \nu = 0, 1, 2 \ldots 2m - 1 \tag{26a}$$

and

$$\vartheta_2 = \frac{1}{m}\operatorname{arsinh}\frac{q}{\epsilon} \tag{26b}$$

The location of the zeros is, with Eq. (24), $s = j \cos \vartheta = j \cos(\vartheta_1 + j\vartheta_2)$ or

$$s = \sin\vartheta_1 \sinh\vartheta_2 + j\cos\vartheta_1 \cosh\vartheta_2 = \beta + j\gamma \tag{26c}$$

This finally provides

$$\frac{\beta^2}{\sinh^2\vartheta_2} + \frac{\gamma^2}{\cosh^2\vartheta_2} = \sin^2\vartheta_1 + \cos^2\vartheta_1 = 1 \tag{27}$$

The zeros obviously lie on an ellipse, as shown for $m = 3$ in Fig. 14. Finally,

$$K(s) = \pm\epsilon\, 2^{m-1}\prod_{i=1}^{m}(s - s_i) \tag{28a}$$

or

$$F(s) = \frac{\pm 1}{\epsilon\, 2^{m-1}\prod_{i-1}^{m}(s - s_i)} \tag{28b}$$

represents the solution for the desired $K(s)$ and $F(s)$ with the m zeros of Eq. (22b) and the coefficient of the leading term stemming from the Chebyshev polynomial in Eqs. (14) and (15).

Determination of the Chain Matrix A and of $f(s)$. The chain matrix of the lossless two-port in Fig. 1 is

$$A = \begin{pmatrix} A_{11} & A_{12} \\ A_{21} & A_{22} \end{pmatrix} \tag{29}$$

with

$$\begin{pmatrix} V_1 \\ I_1 \end{pmatrix} = A \begin{pmatrix} V_2 \\ I_2 \end{pmatrix} \tag{30}$$

Necessary and sufficient conditions for a realizable LC chain matrix are as follows (17):

1. The four elements of A are rational in s and real for real s. A_{11} and A_{22} are even, and A_{12}, A_{21} are odd functions of s.
2. $\det A = 1$.
3. At least three ratios of horizontally or vertically adjoining elements are LC driving point impedances. For $A_{12} \equiv 0$ or $A_{21} \equiv 0$ or $A_{12}, A_{21} \equiv 0$, the elements A_{11} and A_{22} are constants reciprocal to each other.

$K(s)$ can be expressed as

$$K(s) = \frac{V_0}{V_2} = \left(A_{11} + \frac{A_{12}}{R_2} + \left(\frac{q}{2}\right)^2 (R_2 A_{21} + A_{22})\right) \quad \text{with } q = 2\sqrt{\frac{R_1}{R_2}} \tag{31}$$

The term q is explained in Eq. (2). With an unknown "characteristic" function $f(s)$, we obtain

$$A_{11} + \frac{A_{12}}{R_2} = \frac{1}{2}(K(s) + f(s)) \tag{32a}$$

and

$$\left(\frac{q}{2}\right)^2 (A_{22} + R_2 A_{21}) = \frac{1}{2}(K(s) - f(s)) \tag{32b}$$

According to condition 1, A_{11}—respectively, $(q/2)^2 A_{22}$—are the even parts of 1/2 ($K(s) + f(s)$)—respectively, 1/2 ($K(s) - f(s)$). A_{12}/R_2—respectively, $(q/2)^2\, R_2 A_{21}$—are the odd parts of 1/2 ($K(s) + f(s)$)—respectively, 1/2 ($K(s) - f(s)$). This provides

$$A_{11} = \frac{1}{4}(K(s) + f(s) + K(-s) + f(-s)) \tag{33a}$$

$$\frac{A_{12}}{R_2} = \frac{1}{4}(K(s) + f(s) - K(-s) - f(-s)) \tag{33b}$$

$$\left(\frac{q}{2}\right)^2 A_{22} = \frac{1}{4}(K(s) - f(s) + K(-s) - f(-s)) \tag{33c}$$

$$\left(\frac{q}{2}\right)^2 R_2 A_{21} = \frac{1}{4}(K(s) - f(s) - K(-s) + f(-s)) \tag{33d}$$

From $\det A = 1$, we derive

$$A_{11}\left(\frac{q}{2}\right)^2 A_{22} - \frac{A_{12}}{R_2}\left(\frac{q}{2}\right)^2 R_2 A_{21} = \left(\frac{q}{2}\right)^2$$

or, with Eqs. (33a) through (33d),

$$K(s)K(-s) - q^2 = f(s)f(-s), \qquad \text{with } q = 2\sqrt{R_1/R_2} \tag{34}$$

As $K(s)$ and q^2 are known, $f(s)$ can be determined by the same consideration as applied for finding $K(s)$. The product $f(s)f(-s)$ is even; its zeros are assigned in complex conjugate pairs, if complex, to $f(s)$ and the location with the opposite sign to $f(-s)$. The constraint of stability, mandatory for $K(s)$, does not apply for $f(s)$ as $f(s)$ is no insertion voltage loss.

For Chebyshev filters we obtain, from Eqs. (22a), (22b), and (34),

$$f(s)f(-s) = \epsilon^2 T_m^2\left(\frac{s}{j}\right) = 0 \tag{35}$$

The zeros can be derived from Eqs. (23), (26a), and (26b) for $q/\epsilon = 0$, yielding

$$\vartheta_1 = \frac{2\nu+1}{m}\frac{\pi}{2} \tag{36a}$$

and

$$\vartheta_2 = 0 \tag{36b}$$

with the zeros in Eq. (26c) as

$$s_k = j\cos\vartheta_1 = j\cos\frac{2\nu+1}{m}\frac{\pi}{2}$$
$$\nu = 0, 1 \ldots 2m-1 \text{ and hence } k = 1, 2 \ldots 2m \tag{37a}$$

These zeros on the imaginary axis are double as demonstrated in Fig. 14 for $m = 3$.

Finally, from Eq. (35) we obtain

$$f(s) = \pm\epsilon\, 2^{m-1}\prod_{k=1}^{m}(s - s_k)$$

where s_k are half the zeros in Eq. (35) and where a single zero is taken from each location.

Now the elements A_{ik} of the chain matrix can be calculated using Eqs. (33a) through (33d). There are four possibilities to calculate A depending on the selection of the signs for $K(s)$ and $f(s)$.

Development of an LC Two-Port. Starting with a chain matrix A with known elements A_{ik}, the steps leading to an LC two-port embedded in the resistances R_1 and R_2 in Fig. 1 will be given and explained. The basic concept is the development of an LC reactance function into an LC circuit in such a way that the poles of $K(s)$ are realized. The poles of $K(s)$ in Eq. (31) are the zeros of the denominator and the $n - m$ poles at $s = \infty$ that occur if the degree n of the numerator exceeds the degree m of the denominator, manifested by $n - m > 0$. For an all-pole filter, $K(s)$ is a polynomial where all poles lie at $s = \infty$. The Chebyshev filter is an example of an all-pole filter as well as the Butterworth filter or the Thomson filter, which are treated later.

The development of A into an LC two-port starts with the selection of an element A_{ikL} with the largest degree in s. If there is more than one such element any one may be chosen, yielding different solutions with the same inverse transfer function $K(s)$. Then we form the ratio $D = A_{ikL}/A_{ikN}$ or the inverse $D = A_{ikN}/A_{ikL}$, where A_{ikN} is the element horizontally or vertically next to A_{ikL}. The ratios are LC two-terminal functions. There are four possibilities to form them depending on the selection of the neighbor to A_{ikL}. Together with the four possible chain matrices, we are at this point already faced with at least 16 possible LC one-ports, with every one ensuring an equivalent solution.

The ratios may represent either an input or an output driving point impedance function with a short circuit or an open circuit at the receiving end. The short circuit or the open circuit is later replaced either by the load R_2 or the input voltage V_0 with the resistance R_1 depending on the physical meaning of the two-terminal function.

The development of the LC driving point impedance function is based on a modified continued fraction expansion (16a,16b) with partial pole removals (18–20) only allowed at poles of $K(s)$ and preferably at those poles of $K(s)$ at $s = \infty$ or $s = 0$. The process is explained by the pole-zero plot in Fig. 15. The headline shows the poles of $K(s)$ to be realized. A full circle ○ or cross mark × stands for the two zeros or the two poles at $s = \pm j\Omega$ and for the associated degree 2 in s, whereas a half circle ∩ or a half cross mark ∨ stands for the degree 1 in s. We assume that Y in the second line is the admittance D we have chosen from the chain matrix. The partial fraction to the pole at $s = 0$ is a_0/s. We remove part of this pole by subtracting a_1/s with $a_1 < a_0$. It can be shown (16a,16b) that

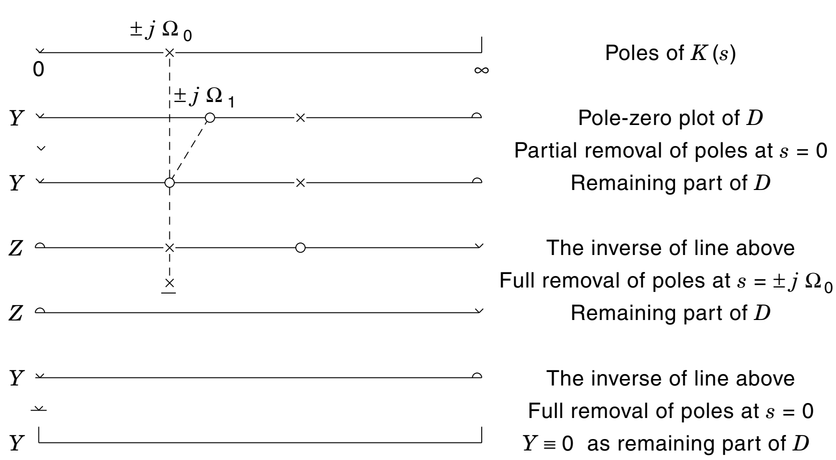

Figure 15. Pole-zero plot of D with admittances Y and impedances Z during partial ∨ and full $\underline{\times}$ removal of poles.

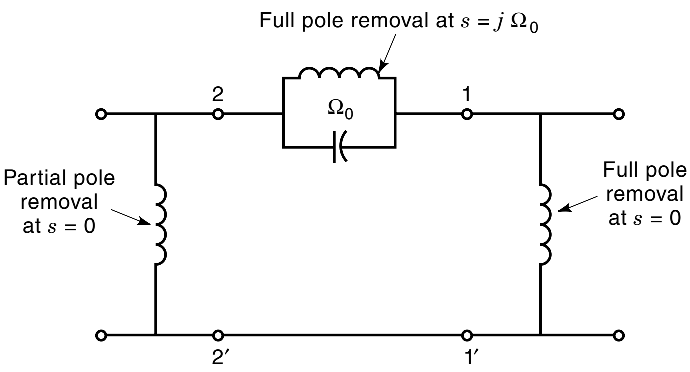

Figure 16. *LC* two-port generated by the development in Fig. 15.

by doing this all zeros beside the one at $s = \infty$ move toward the pole partially removed. a_1 is chosen such that the zero at $s = j\Omega_1$ moves to $s = j\Omega_0$. a_1/s is realized by the first inductor in Fig. 16. A proof that there is always an $0 < a_1 < a_0$ able to generate the desired zero is missing. Now the admittance Y is inversed, and the pole of the impedance Z at $s = j\Omega_0$ is fully removed ($\times$) and realized by the series parallel resonator in Fig. 16. The two-port shall exhibit a transmission zero at $s = j\Omega_0$ because the infinite impedance of the series parallel resonator prevents energy from being delivered into the resistor R_2, which hence exhibits a zero voltage at frequency Ω_0. The same is true for a shunt zero impedance. It is even true for a series infinite impedance or a shunt zero impedance, which are generated by a partial pole removal, because these impedances block the energy transfer to the output resistance R_2. This imposes the constraint that a partial pole removal is only allowed at poles of $K(s)$.

The partial removal of a pole does not lower the degree of the driving point function. As a consequence, the two-port generated does not exhibit the minimum number of components. To minimize the number of components, partial pole removal preferably should take place at $s = 0$ or $s = \infty$, as it is there associated with only one reactance.

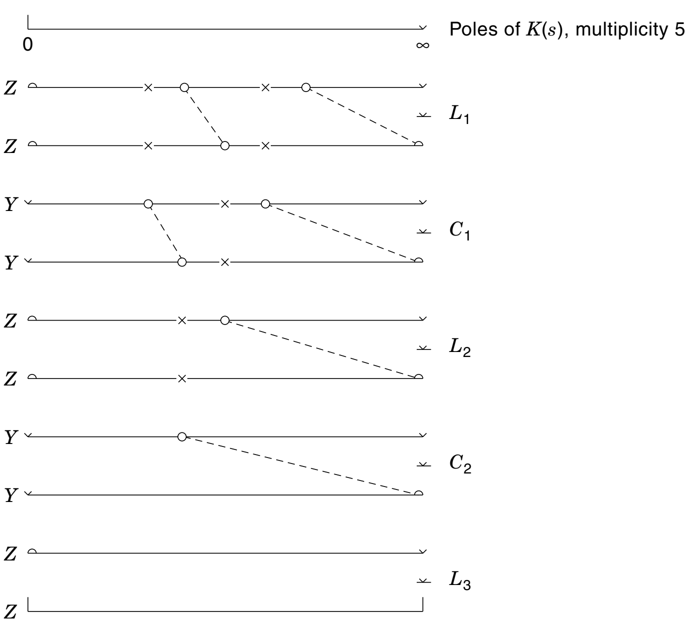

Figure 17. Always in full pole removal $\underline{\vee}$ if $K(s)$ is a polynomial in s; Y = admittances, Z = impedances.

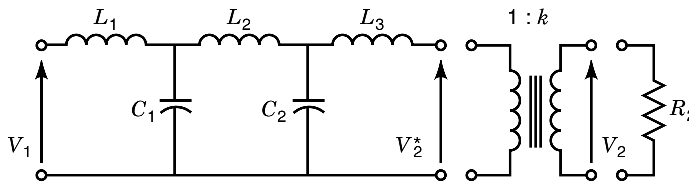

Figure 18. An *LC* two-port if $K(s)$ is a polynomial.

So far, the procedure for rational functions D has been described. The function $K(s)$ of Chebyshev filters in Eq. (28a) is a polynomial where all poles lie at $s = \infty$. The development of the *LC* two-port is a special case plotted in Figs. 17 and 18 (16c). We start with an impedance, the pole of which at $s = \infty$ is fully removed, realizing a pole of $K(s)$ at $s = \infty$ by the inductor L_1 in Fig. 18. The full pole removal in the admittance of the next step provides the shunt capacitor C_1 realizing another pole at $s = \infty$. The process continues in Figs. 17 and 18 (16c) until all poles are realized by three inductors and two capacitors. Since for the Chebyshev filter only full pole removals were used, the circuit generated exhibits the minimum number of components.

So far, from the given matrix A in Eq. (29), the matrix A^* in Eq. (37b)

$$A^* = \begin{pmatrix} kA_{11} & A_{12}^* \\ kA_{21} & A_{22}^* \end{pmatrix} \tag{37b}$$

is realized if we assume that the driving point function D was selected as $D = A_{11}/A_{21}$. In D a common constant factor k may have been canceled. The physical meaning of A_{11} is $A_{11} = V_1/V_2$ for $I_2 = 0$ and of $A_{11}^* = kA_{11} = V_1/V_2^*$ for $I_2^* = 0$, where V_2^* (respectively, I_2^*) are the output voltage (respectively, current) in Fig. 19 at the *LC*-two-port A^* so far realized. The terms are evaluated at an arbitrarily chosen frequency, where $s_0 = 0$ or $s_0 = \infty$ are especially easy to handle. The result is $k = A_{11}^*(s_0)/A_{11}(s_0)$. The correction for $k \neq 1$ is achieved by an ideal transformer in Fig. 19 with matrix T in cascade with A^* providing

$$A^*T = \begin{pmatrix} kA_{11} & A_{12}^* \\ kA_{21} & A_{22}^* \end{pmatrix} \begin{pmatrix} \frac{1}{k} & 0 \\ 0 & k \end{pmatrix} = \begin{pmatrix} A_{11} & kA_{12}^* \\ A_{21} & kA_{22}^* \end{pmatrix} \tag{37c}$$

We claim that with this last step the given matrix A is realized. For proof we consider for the matrices A and A^*T the equations

$$\det A = A_{11}A_{22} - A_{12}A_{21} = 1$$

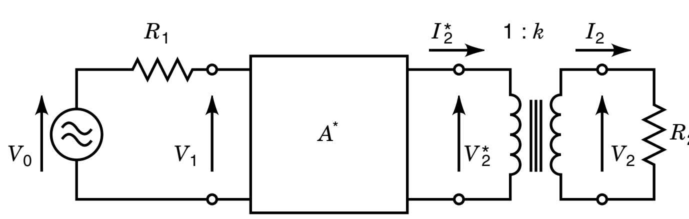

Figure 19. The intermediate steps A^*, the ideal transformer, and the embedding in R_1 and R_2 during the synthesis of two-ports.

and

$$\det A^*T = A_{11}kA^*_{22} - kA^*_{12}A_{21} = 1$$

The poles of $K(s)$ are given by the denominators of the elements A_{ik} according to Eq. (31). They are already realized by the synthesis procedure and are equal in A and A^*. Therefore, we now concentrate on the numerators of A_{ik}. We assume that A_{11} has the highest degree in s. At the n zeros of A_{11} we obtain $A_{12} = -1/A_{21}$ and $kA^*_{12} = -1/A_{21}$. That means that the numerators of A_{12} and kA^*_{12} of degree $<n$ are identical at n points; hence they are identical for all s. The same applies to A_{22} and kA^*_{22}. Therefore, $A^*T = A$, as desired.

Some remarks about the procedure for synthesizing an LC two-port are necessary:

1. As mentioned previously, a proof has not yet been found that partial pole removal with positive value of the components is always feasible. However, so far there has always been a realizable two-port among all the alternatives for equivalent solutions.
2. If in each element in A the common factors are canceled, then it can be proved that horizontally or vertically adjoining elements exhibit no common zeros. However, for some developments it is necessary to represent all elements with one single common denominator. Then common zeros of adjoining elements may occur. They are also zeros of $K(s)$ and are realized by a partial fraction expansion. The pertinent circuits are added in series of an open circuit reactance function and in the shunt of a short circuit reactance function D. This brief remark may suffice.
3. The alternative solutions can differ in the number of inductors and capacitors. Hence a search for a circuit with the minimum number of inductors is worthwhile because capacitors are, as a rule, less costly.
4. Developments with capacitors connected to a common terminal, such as ground, are advantageous since parasitic capacitances can be included in these capacitors.
5. Tuning of the transmission zeros can be carried out by adjusting one element, preferably the capacitor, in the series or parallel resonators.
6. The procedure can be used to generate specific one-ports such as the equivalent circuit for a quartz oscillator in Fig. 20.

The general procedure for the synthesis of an LC filter embedded in R_1 and R_2 from a given $|K(j\omega)|^2$ was presented with Chebyshev filters as an example. The procedure shall be applied to all further filters discussed in this article.

Further Filters Derived from Chebyshev Polynomials. In the previous section a low-pass was derived from the squared Chebyshev polynomials $T^2_m(\Omega)$, $\Omega = \omega/\omega_c$. Further filters are generated from $1/T^2_m(\Omega)$, $T^2_m(1/\Omega)$, and $1/T^2_m(1/\Omega)$. These functions are depicted in Figs. 21(a) through 21(c). In the Figs. 22(a) through 22(c) the pertaining filters and their $K(s)$ are shown. It can be seen that a highpass with Chebyshev behavior in the stopband [Fig. 22(a)], a highpass with Chebyshev behavior in the passband [Fig. 22(b)], and a low-pass with Chebyshev behavior in the stopband [Fig. 22(c)] can be generated.

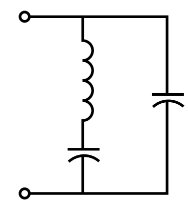

Figure 20. Equivalent circuit of a quartz oscillator.

The Butterworth Approximation (9). Contrary to the Chebyshev approximation, the normalizing frequency usually

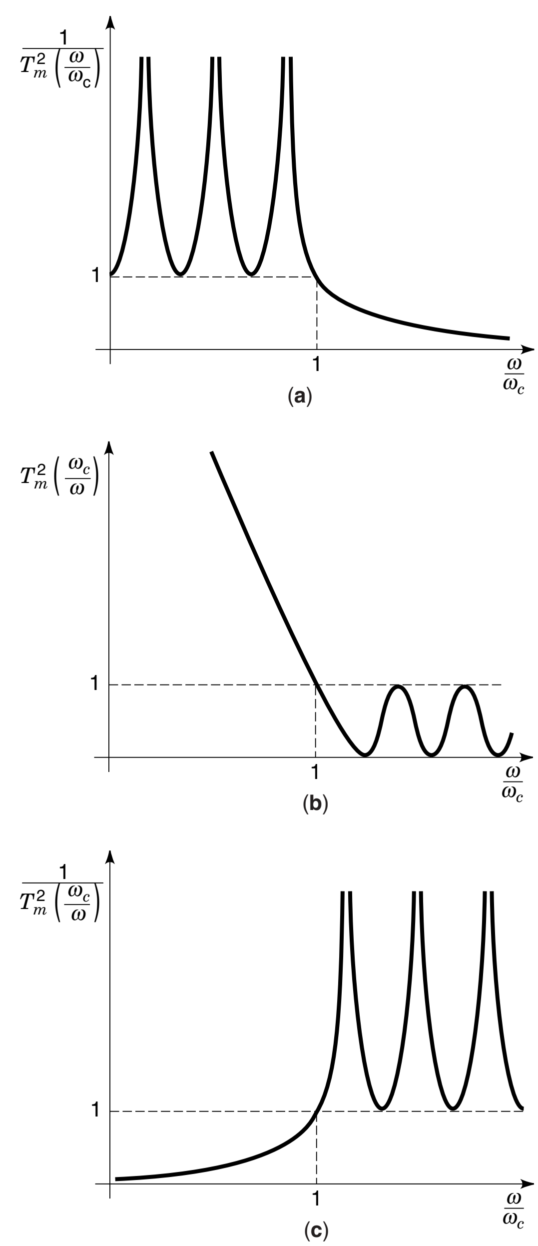

Figure 21. (a) The polynomial $T_m^{-2}(\omega/\omega_c)$. (b) The polynomial $T^2_m(\omega_c/\omega)$. (c) The polynomial $T_m^{-2}(\omega_c/\omega)$.

chosen for the Butterworth filters is ω_c^*, the 3 dB frequency, yielding $\Omega = \omega/\omega_c^*$. We again work with the function $K(j\Omega)$ instead of $F(j\Omega) = K(j\Omega)^{-1}$.

The function

$$|K(j\Omega)|^2 = A_0(1+\Omega^{2n}) = P(\Omega) \geq q^2 = 4R_1/R_2 \qquad (38)$$

exhibits $d^\nu P(\Omega)/d\Omega^\nu = 0$ for $\Omega = 0$ and $\nu = 1, 2, \ldots 2n-1$ and is hence maximally flat at $\Omega = 0$.

The inequality in Eq. (38) is met for $A_0 \geq q^2$. $|K(j\Omega)|$ and $|F(j\Omega)| = |K(j\Omega)|^{-1}$ are plotted in Fig. 23. The 3 dB cutoff frequency is reached at $\Omega = 1$. For large $\Omega \gg 1$, we obtain $|K(j\Omega)| \approx \sqrt{A_0}\Omega^n$ and the attenuation $a(\Omega) = 20 \log |K(j\Omega)| \approx 20n \log \Omega + 20 \log \sqrt{A_0}$, from which an increase in attenuation Δa for one frequency decade of $\Delta a = n \cdot 20$ dB/decade can be seen.

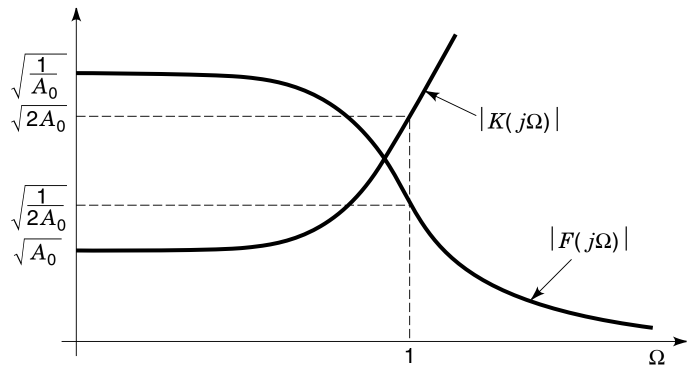

Figure 23. The magnitude $|F(j\Omega)|$ of the transfer function and the magnitude $|K(j\Omega)|$ of the inverse transfer function for Butterworth filters.

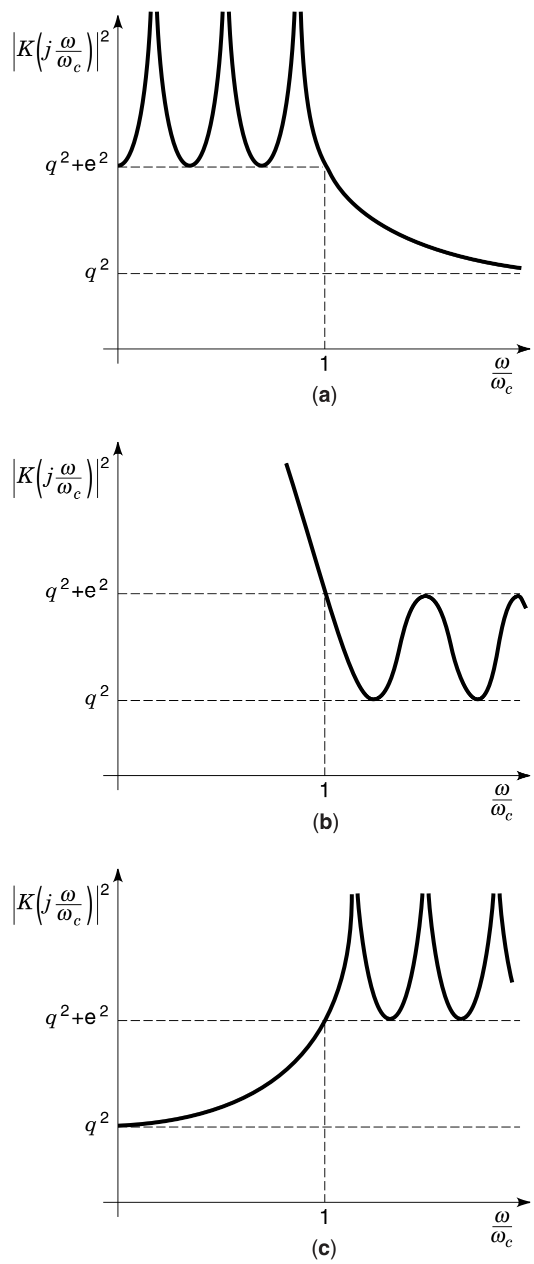

Figure 22. (a) The highpass with $|K(j(\omega/\omega_c))|^2 = q^2 + \epsilon^2\, T_m^{-2}(\omega/\omega_c)$ and Chebyshev behavior in the stopband. (b) The highpass with $|K(j(\omega/\omega_c))|^2 = q^2 + \epsilon^2\, T_m^2(\omega_c/\omega)$ and Chebyshev behavior in the passband. (c) The lowpass with $|K(j(\omega/\omega_c))|^2 = q^2 + \epsilon^2\, T_m^{-2}(\omega_c/\omega)$ and Chebyshev behavior in the stopband.

According to Eq. (38), we obtain

$$Q(s) = P\left(\frac{s}{j}\right) = A_0(1+(-1)^n s^{2n}) = K(s)K(-s) \qquad (39)$$

The zeros of $Q(s)$ are given by $s^{2n} = (-1)^{n-1} = e^{j\pi(n-1+2k)}$ for $k = 0, 1, 2, \ldots, 2n-1$. This yields the zeros

$$s_k = e^{j\frac{\pi}{2n}(n-1+2k)} \qquad (40)$$

Obviously, the zeros lie on the unit circle of the complex s-plane. If they are complex, they have to be complex conjugate, as $Q(s)$ possesses only real coefficients. For $n = 4$ the zeros are plotted in Fig. 24. The zeros in Re $s < 0$ are assigned to $K(s)$, yielding a stable two-port. For $n = 4$ we obtain

$$K(s) = \pm\sqrt{A_0}\left(s - e^{j\,5\pi/8}\right)\left(s - e^{-j\,5\pi/8}\right)\left(s - e^{j\,7\pi/8}\right)\left(s - e^{-j\,7\pi/8}\right)$$

or

$$K(s) = \pm\sqrt{A_0}(s^4 + 2.613s^3 + 3.414s^2 + 2.613s + 1)$$

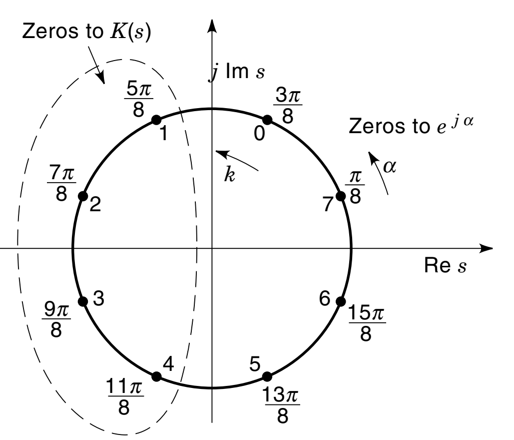

Figure 24. The zeros of $Q(s) = K(s)K(-s)$ in Eq. (39) of Butterworth filters for $n = 4$.

Table 3. Polynomials $K(s)$ for Butterworth Filters.

n	$K(s)/\sqrt{A_0}$
1	$s + 1$
2	$s^2 + \sqrt{2}s + 1$
3	$s^3 + 2s^2 + 2s + 1$
4	$s^4 + 2.613s^3 + 3.414s^2 + 2.613s + 1$

Table 3 lists $K(s)/\sqrt{A_0}$ for Butterworth filters with degree n = 1 through n = 4.

The characteristic polynomial is determined due to Eq. (34) by

$$K(s)K(-s) - q^2 = f(s)f(-s) \tag{41}$$

or

$$A_0(1 + (-1)^n s^{2n}) - q^2 = f(s)f(-s) \tag{42}$$

The zeros are given by

$$s^{2n} = (-1)^{n-1}\left(1 - \frac{q^2}{A_0}\right)$$

or

$$s_r = \left(1 - \frac{q^2}{A_0}\right)^{1/2n} e^{j\frac{\pi}{2n}(n-1+2k)} \tag{43}$$

where $k = 0, 1, \ldots 2n - 1$ and hence $r = 1, 2, \ldots 2n$.

The $2n$ zeros lie on a circle in the s-plane with radius

$$r_0 = \left(1 - \frac{q^2}{A_0}\right)^{1/2n}$$

and are complex conjugate or real. Any complex conjugate pair and any real zero can be assigned to $f(s)$, while the negative locations of these zeros belong to $f(-s)$. This yields

$$f(s) = \pm\sqrt{A_0}\prod_{r=1}^{n}(s - s_r)$$

With $K(s)$ and $f(s)$ now known, the elements of the chain matrix are calculated by Eqs. (33a) through (33d), followed by the development of the matrix into a two-port with the procedure outlined previously. As an example, the solution for the chain matrix A and for the pertaining two-port is now listed for $n = 3$, $A_0 = 1$, and $R_1 = R_2$:

$$A_{11} = 2s^2 + 1; \qquad A_{12} = R_2(2s^3 + 2s);$$
$$A_{21} = \frac{2s}{R_2}; \qquad A_{22} = 2s^2 + 1$$

As all elements are polynomials in s, the pertaining two-port in Fig. 25 was found by full pole removals and therefore exhibits the minimum number of components.

The solution, based on the normalized frequency $\Omega = \omega/\omega_c^*$, provides the normalized values for the components l_1, l_2, and c in Fig. 25, where the denormalized values L_1, L_2, and C are also listed.

The Thomson or Bessel Approximation (11). A filter with a linear phase $\psi(\omega) = \omega t_0$ provides an ideal delay by t_0 and exhibits the function

$$K\left(j\frac{\omega}{\omega_0}\right) = ae^{j\frac{\omega}{\omega_0}\omega_0 t_0}$$

With $\omega_0 t_0 = 1$ and $\Omega = \omega/\omega_0$ we obtain for $s = j\Omega$ extended into the s-plane

$$K(s) = ae^s \tag{44}$$

This normalization with ω_0 is different from the one used previously for the comparison of $a(t)$. It is commonly used and emphasizes the delay $t_0 = 1/\omega_0$ as the most important property of Bessel filters.

The group delay $d\psi/d\omega = t_0$ is a constant. We have to approximate the filter with constant group delay by a realizable function $K(s)$. A Taylor series for e^s is no more Hurwitz from the fifth-order term on. A realizable solution is provided by setting $K(s) = ae^s = a(\cosh s + \sinh s)$, where

$$\cosh s = 1 + \frac{s^2}{2!} + \frac{s^4}{4!} + \ldots \tag{45a}$$

is an even function and

$$\sinh s = s + \frac{s^3}{3!} + \frac{s^5}{5!} + \ldots \tag{45b}$$

is an odd function in s.

A theorem states that if the ratio of the even part of a polynomial over the odd part is an LC driving point function and if the even and odd parts are coprime, then the sum of the even and odd parts is Hurwitz. To check the property of an LC driving point impedance function, we develop the continued fraction based on Eqs. (45a) and (45b).

$$\frac{\cosh s}{\sinh s} = \frac{1}{s} + \cfrac{1}{\cfrac{3}{s} + \cfrac{1}{\cfrac{5}{s} + \cfrac{1}{\cfrac{7}{s} + \ldots \cfrac{1}{\cfrac{2N-1}{s} + \ldots}}}} = \frac{m(s)}{n(s)} \tag{46}$$

Since all terms in the infinite continued fraction expansion are positive, $h(s) = m(s) + n(s)$ calculated from Eq. (46) trun-

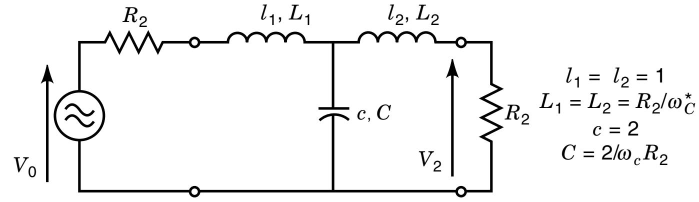

Figure 25. The Butterworth filter for $n = 3$, $A_0 = 1$, and $R_1 = R_2$.

Table 4. A List of Modified Bessel Polynomials $B_\nu(s)$ and Their Factored Form for ν up to 5.

$B_0(s) = 1$
$B_1(s) = s + 1$
$B_2(s) = s^2 + 3s + 3$
$B_3(s) = s^3 + 6s^2 + 15s + 15 = (s + 2.322)(s^2 + 3.678s + 6.460)$
$B_4(s) = s^4 + 10s^3 + 45s^2 + 105s + 105 = (s^2 + 5.792s + 9.140) \times (s^2 + 4.208s + 11.488)$
$B_5(s) = s^5 + 15s^4 + 105s^3 + 420s^2 + 945s + 945 = (s + 3.647)(s^2 + 6.704s + 14.272)(s^2 + 4.679s + 18.156)$

cated at $(2N - 1)/s$ is Hurwitz. For $2N - 1 = 7$, we obtain from Eq. (46)

$$\frac{m(s)}{n(s)} = \frac{s^4 + 45s^2 + 105}{10s^3 + 105s} \text{ and } K(s) = aC[m(s) + n(s)]$$
$$= aC(s^4 + 10s^3 + 45s^2 + 105s + 105)$$

The factor C is needed to render $K(0) = a$, as required by Eq. (44). In the example $C = 1/105$, $m(s) + n(s)$ can be expressed by modified Bessel polynomials:

$$B_\nu(s) = s^\nu B_\nu^*\left(\frac{1}{s}\right) = m(s) + n(s) \tag{47a}$$

with

$$B_\nu^*\left(\frac{1}{s}\right) = \sum_{k=0}^{\nu} \frac{(\nu + k)!}{(\nu - k)!\,k!\,(2s)^k} \tag{47b}$$

A recursion formula is given by

$$B_\nu(s) = (2\nu - 1)B_{\nu-1}(s) + s^2$$

$B_{\nu-2}(s)$. With Eqs. (47a) and (47b),we finally obtain

$$K(s) = a\,B_\nu(0)^{-1} B_\nu(s) \tag{48}$$

Table 4 lists the Bessel polynomials up to $\nu = 5$ (4).

The constant a is chosen such that the constraint for $|K(j\Omega)|$ is met. The characteristic function is determined by $K(s)K(-s) - q^2 = f(s)f(-s)$. The LC two-port is then calculated by the procedure given previously, applied for polynomials.

Cauer Filters (4,12,21). These filters exhibit Chebyshev behavior in the passband and in the stopband, as depicted in Fig. 26. They are based on elliptic functions as derived by Cauer and are therefore also called elliptic filters. The theory of elliptic filters is very involved. A simpler approach based on the results is given here.

The filter function in Fig. 26 is represented by

$$|K(j\Omega)|^2 = q^2 + \epsilon^2 F_n^2(\Omega) \tag{49}$$

with

$$F_n(\Omega) = \begin{cases} k \displaystyle\prod_{\nu=1}^{n/2} \frac{\Omega^2 - \Omega_\nu^2}{\Omega^2 - (\Omega_s/\Omega_\nu)^2} & n \text{ even} \quad (50) \\ k\Omega \displaystyle\prod_{\nu=1}^{(n-1)/2} \frac{\Omega^2 - \Omega_\nu^2}{\Omega^2 - (\Omega_s/\Omega_\nu)^2} & n \text{ odd} \quad (51) \end{cases}$$

The equiripple behavior of $F_n^2(\Omega)$ in $\Omega \in [0, 1]$ in Fig. 27 is guaranteed by the choice of Ω_ν according to

$$\Omega_\nu = \begin{cases} \operatorname{sn}\left(\dfrac{E\left(\frac{1}{\Omega_s}\right)(2\nu - 1)}{n}\right) & n \text{ even}, \nu = 1, 2, \ldots \dfrac{n}{2} \quad (52a) \\ \operatorname{sn}\left(\dfrac{E\left(\frac{1}{\Omega_s}\right)2\nu}{n}\right) & n \text{ odd}, \nu = 1, 2, \ldots \dfrac{n-1}{2} \quad (52b) \end{cases}$$

where

$$E\left(\frac{1}{\Omega_s}\right) = \int_0^{\pi/2} \frac{d\phi}{\left(1 - \frac{1}{\Omega_s^2}\sin^2\phi\right)^{1/2}} \tag{53a}$$

is the complete elliptic integral of the first kind and the Jacobi-elliptic function $\operatorname{sn}(u) = \sin\varphi$ is calculated from the inverse $\varphi(u)$ of the incomplete elliptic integral of the first kind:

$$u = \int_0^{\varphi} \frac{d\phi}{\left(1 - \frac{1}{\Omega_s^2}\sin^2\phi\right)^{1/2}} \tag{53b}$$

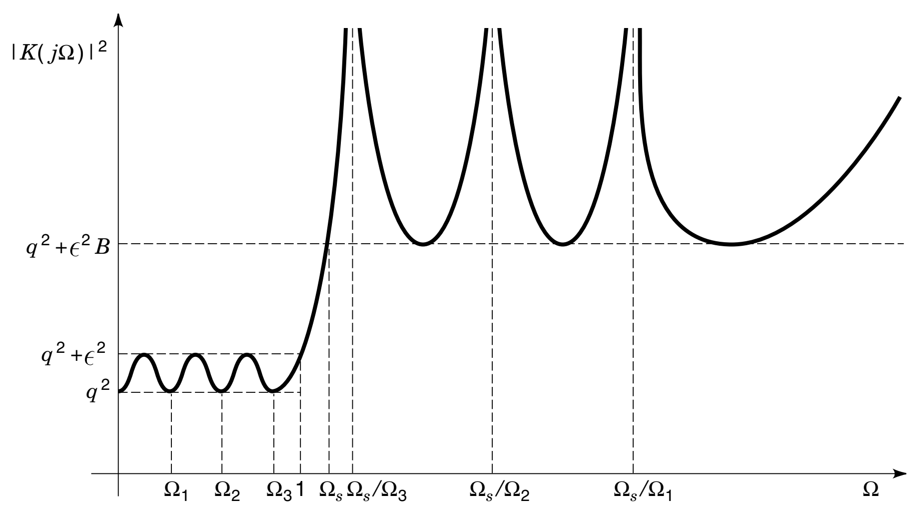

Figure 26. The characteristic $|K(j\Omega)|^2$ of a Cauer filter for n odd in Eq. (49).

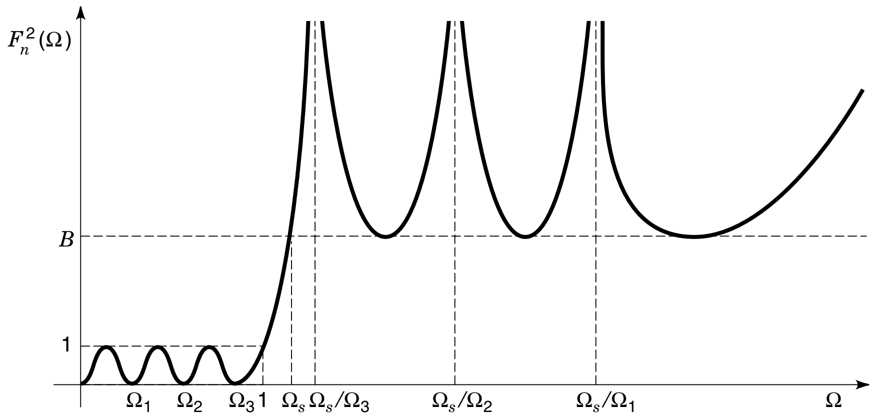

Figure 27. $F_n^2(\Omega)$ for a Cauer filter in Fig. 26 and in Eqs. (50) and (51).

followed by forming $\sin\varphi = \mathrm{sn}(u)$. Ω_s is chosen as $\Omega_s > 1$; Eqs. (52a) and (52b) yield $0 < \Omega_\nu < 1$, $\nu = 1, 2, \ldots n/2$, or $(n-1)/2$. Obviously, the zeros of $F_n^2(\Omega)$ lie in $|\Omega| < 1$ and the poles in $|\Omega| > \Omega_s$. k in Eqs. (50) and (51) is chosen such that $F_n^2(\Omega)$ in Fig. 27 oscillates between 0 and 1 in $\Omega \in [0, 1]$.

Finally, the minimum value B of $F_n^2(\Omega)$ in the stopband in Fig. 27 is given by

$$B = \begin{cases} k\displaystyle\prod_{\nu=1}^{n/2} \frac{\Omega_s^2 - \Omega_\nu^2}{\Omega_s^2 - (\Omega_s/\Omega_\nu)^2} & n \text{ even} \quad (54a) \\ k\Omega_s \displaystyle\prod_{\nu=1}^{(n-1)/2} \frac{\Omega_s^2 - \Omega_\nu^2}{\Omega_s^2 - (\Omega_s/\Omega_\nu)^2} & n \text{ odd} \quad (54b) \end{cases}$$

if the degree n of $F_n(\Omega)$ is chosen as

$$n \geq \frac{E(1/\Omega_s)E(\sqrt{1-1/B})}{E(\sqrt{1/B})E(\sqrt{1-(1/\Omega_s)^2})} \tag{55}$$

If the minimum value for n is not an integer, then the next larger integer has to be chosen. In this case the realized B in Eqs. (54a) and (54b) is larger than the desired B in Eq. (55).

From Eq. (49) and Fig. 27, we derive

$$|K(j1)|^2 = q^2 + \epsilon^2$$

and

$$|K(j\Omega_s)^2 = q^2 + \epsilon^2 B$$

For the filter design the desired R_1 and R_2 yield

$$q = 2\sqrt{\frac{R_1}{R_2}},$$

the desired ripple in the passband provides ϵ, and the minimum $q^2 + \epsilon^2 B$ of $|K(j\Omega)|^2$ in the stop-band yields B in Eqs. (54a) and (54b).

Approximation of $|K(j\Omega)|^2$ by Conformal Mapping (4). Lowpasses with Chebyshev behavior in the passband and arbitrary characteristics in the stopband can be designed by a conformal mapping. This includes also the case of Chebyshev behavior in the passband and the stopband as a special case.

The procedure is based on the fact that the Hurwitz polynomial

$$h(s) = m(s) + n(s) \tag{56}$$

where $m(s)$ is even and $n(s)$ is odd, provides the reactance function $m(s)/n(s)$. It can be further shown that the driving point impedance function

$$w(s) = \frac{m/n}{1 + \dfrac{m}{n}} = \frac{m(s)}{m(s) + n(s)} \tag{57}$$

has the property

$$|w(j\Omega)|^2 = \frac{m^2(j\Omega)}{m^2(j\Omega) - n^2(j\Omega)} \qquad \in [0, 1] \tag{58}$$

for $\Omega \in [-\infty, \infty]$. This shall provide the Chebyshev behavior. We investigate

$$f(z^2) = \frac{m^2(z)}{m^2(z) - n^2(z)} \text{ with } z = u + jv \tag{59}$$

and the transformation

$$z^2 = 1 + \frac{1}{s^2} \tag{60}$$

providing

$$\begin{aligned} f(z^2) &= f\left(1 + \frac{1}{s^2}\right) = g(s^2) \\ &= \frac{m^2\left(\sqrt{1 + \dfrac{1}{s^2}}\right)}{m^2\left(\sqrt{1 + \dfrac{1}{s^2}}\right) - n^2\left(\sqrt{1 + \dfrac{1}{s^2}}\right)} \end{aligned} \tag{61}$$

The properties of the transformation in Eq. (60) are investigated in Figs. 28(a) through 28(e), where the passband $s = j\Omega$ with $|\Omega| \leq 1$, denoted by dashed lines, and the stopband

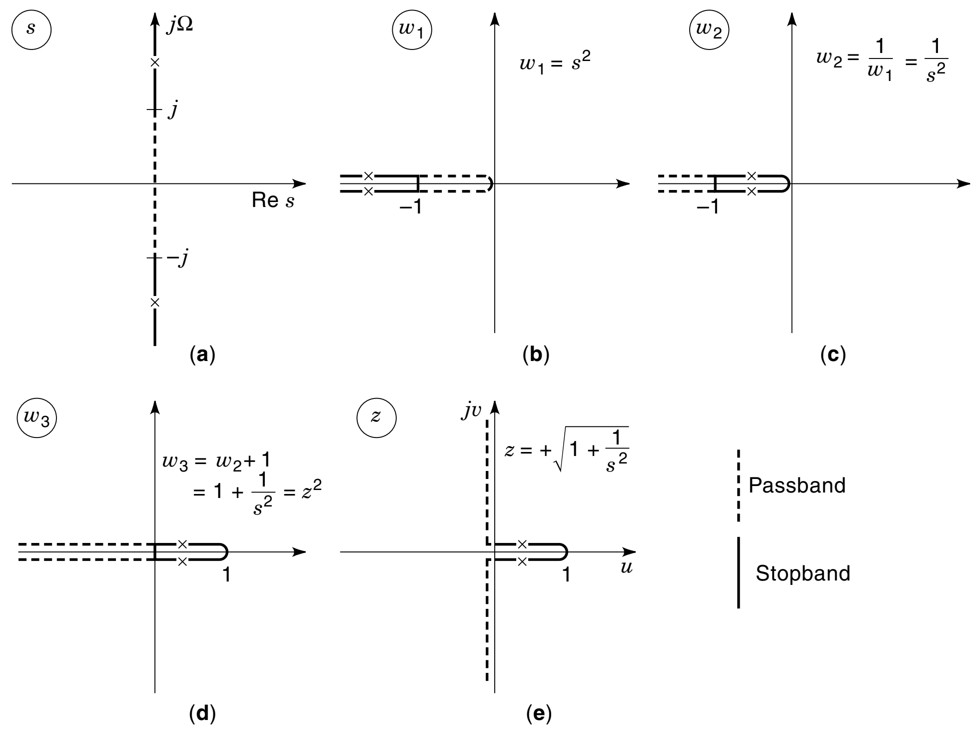

Figure 28. The steps in the conformal mapping $z = +\sqrt{1 + 1/s^2}$ for $s = j\Omega$.

with $|\Omega| \geq 1$, denoted by solid lines, are step by step mapped into the z-plane. The steps from the s-plane to the z-plane in Fig. 28 are $w_1 = s^2$, $w_2 = 1/w_1$, $w_3 = w_2 + 1$, $z = +\sqrt{w_3}$. The result is the following mapping:

$$\Omega \in [-1, 1] \text{ into } v \in [-\infty, \infty] \tag{62a}$$

and

$$|\Omega| \geq 1 \text{ into } u \in [0, 1] \tag{62b}$$

The complex conjugate pair of poles $\times$ in $|\Omega| \geq 1$ results in a double pole in $u \in [0, 1]$. The consequences of this mapping for $f(z^2) = g(s^2)$ in Eqs. (59) and (61) are as follows: for $z = jv$, $v \in [-\infty, \infty]$, and the pertaining $\Omega \in [-1, 1]$:

$$f(-v^2) = g(-\Omega^2) = \frac{m^2(jv)}{m^2(jv) - n^2(jv)} \quad \in [0, 1] \tag{63a}$$

for $z = u$, $u \in [0, 1]$, and the pertaining $|\Omega| \geq 1$ with the constraint $|m(u)| \geq |n(u)|$ and hence

$$0 \leq \frac{n^2(u)}{m^2(u)} \leq 1$$

$$f(u^2) = g(-\Omega^2) = \frac{m^2(u)}{m^2(u) - n^2(u)} = \frac{1}{1 - \dfrac{n^2(u)}{m^2(u)}} \geq 1 \tag{63b}$$

With these results

$$g(-\Omega^2) = \frac{m^2(\sqrt{1 + 1/s^2})}{m^2(\sqrt{1 + 1/s^2}) - n^2(\sqrt{1 + 1/s^2})} \quad \text{for } s = j\Omega$$

assumes the shape in Fig. 29. The function $g(-\Omega^2)$ oscillates between 0 and 1 in the passband as long as $m(s)$ is even and $n(s)$ is odd and $h(s) = m(s) + n(s)$ is Hurwitz. The selection of $m(s)$ and $n(s)$ is the freedom for the design of filters.

For the filter we obtain, as in all previous cases,

$$|K(j\Omega)|^2 = q^2 + \epsilon^2 g(-\Omega^2) \tag{64}$$

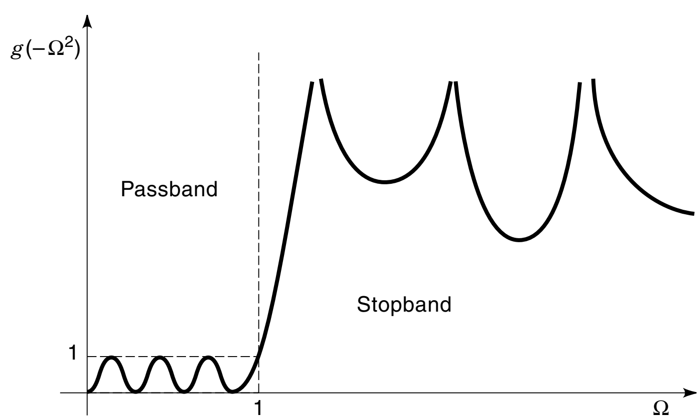

Figure 29. The function $g(-\Omega^2)$ of Eq. (63a) in the passband and the stopband.

with

$$\epsilon^2 g(s^2) = \epsilon^2 \frac{m^2(\sqrt{1+1/s^2})}{m^2(\sqrt{1+1/s^2}) - n^2(\sqrt{1+1/s^2})} \tag{65}$$

or

$$\epsilon^2 g(s^2) = \frac{\epsilon^2}{2}\left[1 + \frac{1}{2}\frac{m+n}{m-n} + \frac{1}{2}\frac{m-n}{m+n}\right] \tag{66}$$

The dominant term in the stop-band, especially around the poles, is

$$|K(j\Omega)|^2 \approx \frac{\epsilon^2}{4}\frac{m(z)+n(z)}{m(z)-n(z)} \tag{67}$$

with $z \in [0, 1]$ and $|\Omega| \geq 1$ in the stopband. The term with the denominator $m(z) + n(z) = h(z)$ in Eq. (66) exhibits no poles in the stopband as $h(z)$ is Hurwitz. Hence the term with the denominator $m(z) - n(z)$ provides the poles. Now we determine m and n from the requirements in the stopband. With the pole locations $z_i \in [0, 1]$ in Eq. (67), which are found later, we obtain

$$m(z) - n(z) = (-z+1)^{\varphi} \prod_{i=1}^{r} (-z+z_i)^2 \tag{68}$$

and by exchanging z with $-z$

$$m(z) + n(z) = (z+1)^{\varphi} \prod_{i=1}^{r} (z+z_i)^2 \tag{69}$$

The term $z = z_i$ in Eq. (68) represents the double pole in $z \in [0, 1]$, while $z = 1$ stands for the pole of multiplicity φ at $\Omega = \infty$. The even part in Eq. (69) provides $m(z)$, whereas the odd part yields $n(z)$. Hence

$$f(z^2) = g(s^2) = \frac{m^2(z)}{m^2(z) - n^2(z)} \tag{70}$$

and $|K(j\Omega)|^2$ in Eq. (67) valid in the stopband are known. The attenuation pertaining to Eqs. (67) through (69) is

$$\begin{aligned} a(\Omega) &= 10\log|K(j\Omega)|^2 \\ &= 20\log\epsilon - 10\log 4 + \sum_{i=1}^{r} 10\log\left(\frac{z+z_i}{-z+z_i}\right)^2 \\ &\quad + \varphi 10\log\frac{(z+1)}{(-z+1)} \end{aligned}$$

The substitution

$$\gamma = \ln z \text{ and } \gamma_i = \ln z_i$$

yields

$$\begin{aligned} r_i &= 10\log\left(\frac{z+z_i}{-z+z_i}\right)^2 = 10\log\left(\frac{e^{\gamma_i}+e^{\gamma}}{e^{\gamma_i}-e^{\gamma}}\right)^2 \\ &= 10\log\left(\frac{e^{\gamma_i-\gamma}+1}{e^{\gamma_i-\gamma}-1}\right)^2 = 20\log\coth\left|\frac{\gamma_i-\gamma}{2}\right| \end{aligned} \tag{71}$$

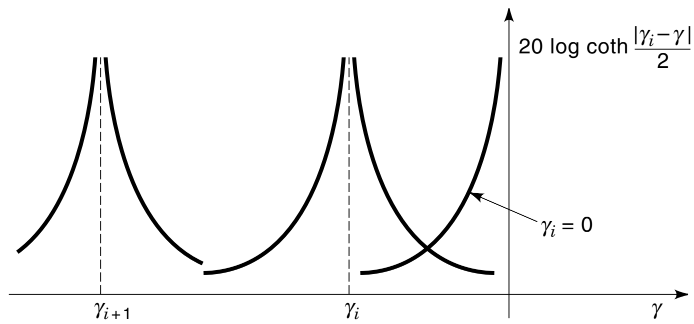

Figure 30. The templates 20 log coth$|\gamma_i - \gamma|/2$ for the approximation of the given characteristics in the stopband.

For $z_i = 1$ we obtain

$$r_\infty = 10\log\left(\frac{z+1}{-z+1}\right)^{\varphi} = 10\varphi\log\coth\frac{|\gamma|}{2} \tag{72}$$

The terms r_i and r_∞ can be considered a template in Fig. 30 that can be shifted to all pole locations $\gamma = \gamma_i$ and $\gamma = 0$.

Any given tolerance scheme in the stopband can be met by a sum of the templates in Eqs. (71) and (72). The number of those templates is minimized by shifting them to appropriate locations γ_i. This numerical search procedure is performed either by a computer program or by trials consisting of shifting and adding templates. The result consists of pole locations z_i, their number r, and the multiplicity φ of the poles at $z = 1$.

As all considerations for the conformal mapping have now been discussed, we are ready to list the sequence of the synthesis steps:

1. The given R_1, R_2 and the ripple in the passband yield q and ϵ.
2. Determine poles z_i.
   a. If only discrete pilot frequencies

   $$z_i = \sqrt{1 - \frac{1}{\Omega_i^2}}$$

   have to be suppressed, then these z_i provide Eq. (68).
   b. If a tolerance scheme in the stopband has to be met, templates provide the pole locations z_i together with r and φ in Eq. (68).
3. Form

$$m(z) - n(z) = (-z+1)^{\varphi} \prod_{i=1}^{r} (-z+z_i)^2$$
$$m(z) + n(z) = (z+1)^{\varphi} \prod_{i=1}^{r} (z+z_i)^2$$

and

$$f(z^2) = g(s^2) = \frac{m^2(\sqrt{1+1/s^2})}{m^2(\sqrt{1+1/s^2}) - n^2(\sqrt{1+1/s^2})}$$

4. Form

$$|K(j\Omega)|^2 = q^2 + \epsilon^2 g(-\Omega^2) = P(\Omega) = P\left(\frac{s}{j}\right) = Q(s)$$

and

$$K(s)K(-s) = Q(s)$$

The zeros and poles of $Q(s)$ provide a stable $K(s)$.

5.

$$f(s)f(-s) = Q(s) - q^2 = \epsilon^2 \frac{m^2(\sqrt{1+1/s^2})}{m^2(\sqrt{1+1/s^2}) - n^2(\sqrt{1+1/s^2})}$$

The zeros and poles of $Q(s) - q^2$ determine $f(s)$.

6. With $K(s)$ and $f(s)$, calculate the elements A_{ik} of the chain matrix and synthesize the LC two-ports embeded in R_1 and R_2.

Transformation of Low-passes Into Other Filters (19). The synthesis procedures presented were all geared to low-passes. The standard approach to generate other filter types is a transformation of the low-pass with frequency variable s and $s = j\Omega$ into a new filter with frequency w and $w = j\lambda$. The general transformation is

$$s = f(w) \tag{73}$$

where $f(w)$ is a reactance function. This will also allow transformation of the reactances Ls and Cs into realizable reactances in the w-domain.

Low-pass Bandpass Transformation. The transformation

$$s = \frac{a}{w} + bw \tag{74}$$

with a, $b > 0$ maps $s = j\Omega$ into $w = j\lambda$ according to

$$\Omega = -\frac{a}{\lambda} + b\lambda \tag{75}$$

as depicted in Fig. 31. The passband of the low-pass with $\Omega \in [-1, 1]$ is translated into the passband with $\lambda \in [\lambda_1, \lambda_2]$ of the bandpass, as indicated by bold lines in Fig. 31. The cutoff frequencies are

$$\lambda_1 = -\frac{1}{2b} + \sqrt{\frac{1}{4b^2} + \frac{a}{b}} \tag{76}$$

$$\lambda_2 = \frac{1}{2b} + \sqrt{\frac{1}{4b^2} + \frac{a}{b}} \tag{77}$$

The center frequency as an image of $\Omega = 0$ is

$$\lambda_0 = \sqrt{\frac{a}{b}} \tag{78}$$

with $\lambda_0^2 = \lambda_1\lambda_2$ representing the geometrical mean of λ_1 and λ_2. The reactances Ls and Cs translate into the series and parallel resonators in Fig. 32. Due to $f(w)$ in Eq. (73) of second degree, a doubling of the reactances is observed. A transformation $f(w)$ of higher degree provides more than one passband, as outlined by the transformation of sixth degree:

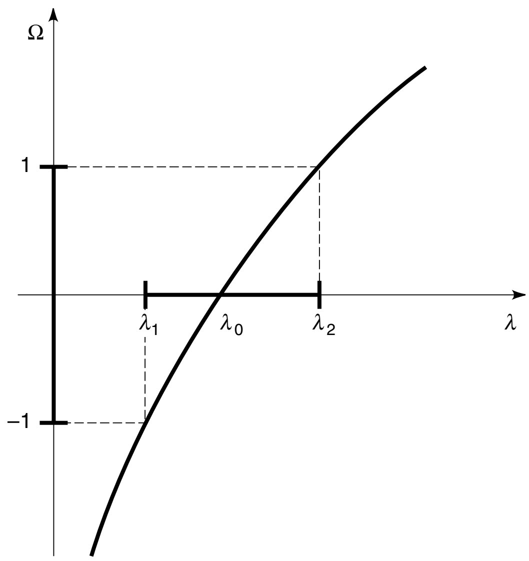

Figure 31. The low-pass bandpass transformation.

$$s = aw + \frac{b}{w} + \frac{cw}{w^2 + \lambda_c^2} + \frac{dw}{w^2 + \lambda_d^2} \tag{79}$$

with a, b, c, d, λ_c^2, λ_d^2, > 0.

The mapping of $s = j\Omega$ into $w = j\lambda$ is shown in Fig. 33, where three passbands are generated. The number of reactances has increased by a factor of 6 due to $f(w)$ of sixth degree.

The Low-pass Bandstop Transformation. For the transformation

$$s = \frac{1}{\dfrac{a}{w} + bw} \qquad \text{with } a, b > 0 \tag{80}$$

the function $\Omega = f(\lambda)$ is shown in Fig. 34 with a stopband for $\lambda \in [\lambda_1, \lambda_2]$ with λ_1, λ_2 and λ_0, as in Eqs. (76) through (78). The doubling of the reactances is demonstrated in Fig. 35.

The Low-pass High-pass Transformation. The transformation

$$s = \frac{a}{w} \tag{81}$$

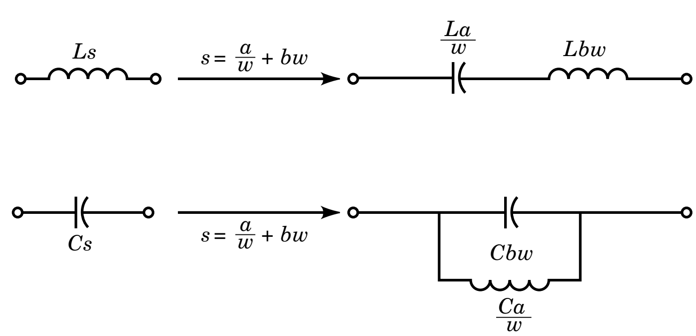

Figure 32. Transformation of reactances for bandpasses.

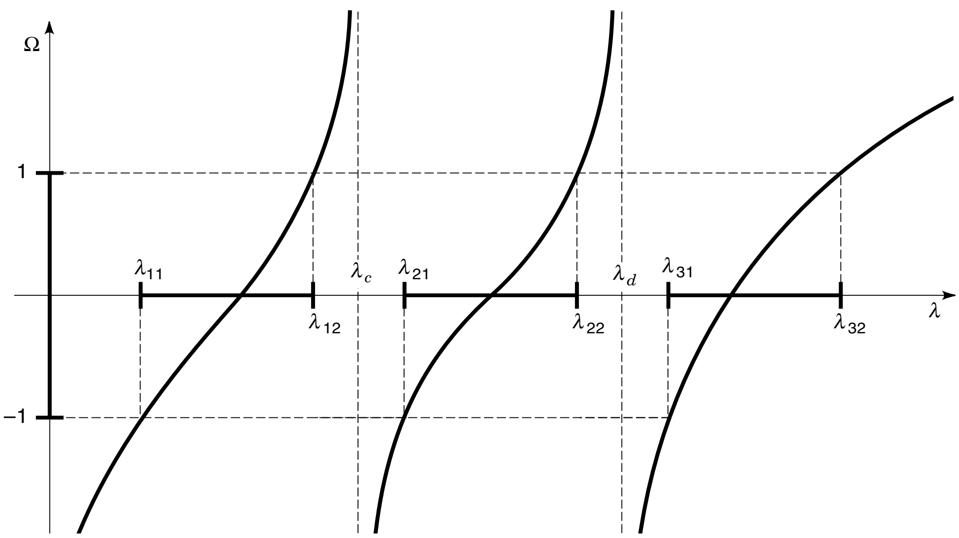

Figure 33. Transformation of a low-pass into a bandpass with multiple passbands.

$a > 0$ yields

$$\Omega = -\frac{a}{\lambda} \tag{82}$$

which is drawn in Fig. 36.

The cutoff frequency of the highpass is

$$\lambda_1 = a \tag{83}$$

According to Fig. 37, inductors and capacitors are interchanged.

Amplitude and Phase Equalizers. Amplitude equalizers generate two-ports with a constant magnitude of the insertion voltage loss function $K(s)$ at least in a limited frequency range. An often encountered solution to this problem is cascading the unequalized two-port with the bridged-T network in Fig. 38. If the impedances Z_1 and Z_2 are chosen according to

$$Z_1 Z_2 = R^2 \tag{84}$$

and if the network is terminated by the resistor R, then the input impedance is also R. This implies that the bridged T terminated by R can replace the load $R_2 = R$ of the original two-port without interaction. The inverse transfer function of the bridged T loaded by R is

$$K_B^*(p) = 1 + \frac{Z_1(p)}{R} \tag{85}$$

For

$$Z_1/R = \frac{1}{G + jY(\omega)}$$

we obtain

$$|K_B^*(j\omega)|^2 = \frac{(1+G)^2 + Y^2(\omega)}{G^2 + Y^2(\omega)}$$

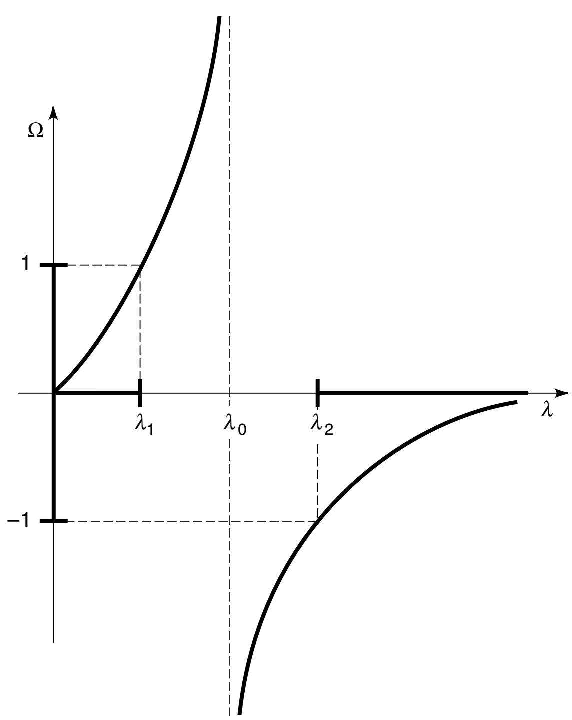

Figure 34. Low-pass bandstop transformation with $\lambda_0 = \sqrt{a/b}$.

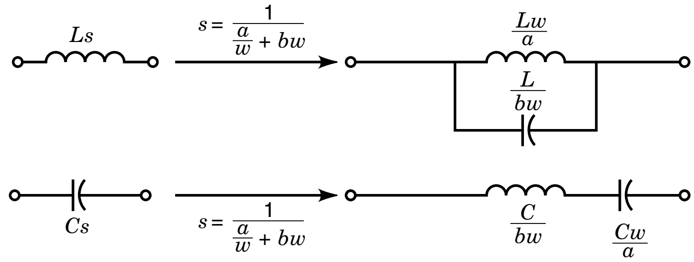

Figure 35. Transformation of reactances for bandstops.

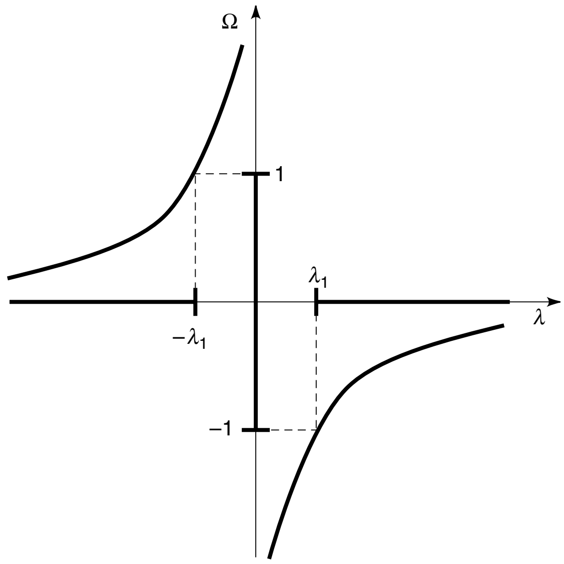

Figure 36. Low-pass high-pass transformation.

and

$$a(\omega) = 10\log\frac{(1+G)^2 + Y^2(\omega)}{G^2 + Y^2(\omega)} \tag{86}$$

The term $a(\omega)$ is the attenuation added to the attenuation of the original two-port in order to equalize the magnitude.

Table 5 lists $a(\omega)$ for various impedances Z_1 and $Z_2 = R^2/Z_1$ (4).

Phase equalizers have the task to provide a linear phase or a constant delay for the equalized two-port. They are commonly allpasses. The inverse transfer function of a first-order and of a second-order allpass are

$$K_1^*(p) = \frac{p+\omega_0}{-p+\omega_0} \tag{87}$$

and

$$K_2^*(p) = \frac{p^2 + \dfrac{2\omega_0}{b}p + \omega_0^2}{p^2 - \dfrac{2\omega_0}{b}p + \omega_0^2} \tag{88}$$

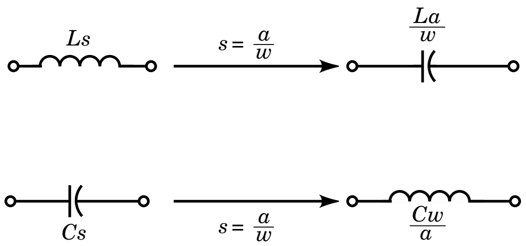

Figure 37. Transformation of reactances for high-passes.

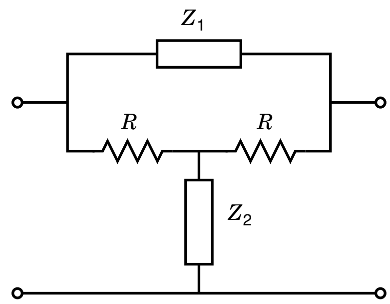

Figure 38. Bridged-T network with $Z_1Z_2 = R^2$ for amplitude equalization.

with the phase $\psi(\omega)$ and the group delay $\tau(\omega)$ as

$$\psi_1(\omega) = \arg K_1(j\omega) = 2\arctan\frac{\omega}{\omega_0}$$

and

$$\psi_2(\omega) = \arg K_2(j\omega) = 2\,\text{arccot}\,\frac{b}{2}\left(\frac{\omega_0}{\omega} - \frac{\omega}{\omega_0}\right)$$

$$\tau_1(\omega) = \frac{d\arg K_1(j\omega)}{d\omega} = \frac{\dfrac{2}{\omega_0}}{1+\left(\dfrac{\omega}{\omega_0}\right)^2} \tag{89}$$

$$\tau_2(\omega) = \frac{d\arg K_2(j\omega)}{d\omega} = \frac{b}{\omega_0}\,\frac{1+\left(\dfrac{\omega_0}{\omega}\right)^2}{1+\left(\dfrac{b^2}{4}\right)\left(\dfrac{\omega}{\omega_0} - \dfrac{\omega_0}{\omega}\right)^2} \tag{90}$$

The group delays $\tau_1(\omega)$ and $\tau_2(\omega)$ are depicted in Figs. 39(a) and 39(b). For $\tau_2(\omega)$ the maximum is approaching $\omega = \omega_0$ depending on increasing values of b. These bell-like curves are added to the nonconstant group delay of the given two-port and thus straighten it out. Several different frequencies ω_0 may be needed for this end. The network in Fig. 40 represents a second-order allpass if it is terminated by R and if the element values are as listed in the figure caption. With the element values given in the figure caption, it exhibits constant input and output impedances and can therefore be cascaded without interaction with the unequalized two-port.

SURFACE ACOUSTIC WAVE FILTERS

Filters for high frequencies in the megahertz or gigahertz range are difficult to realize as the calculation of a three-dimensional electromagnetic field is required. To achieve this, one has to resort to numerical methods, which, as a rule, are inaccurate and hence necessitate complicated tuning of the filters. Filters based on surface acoustic waves (SAW) are somewhat easier to design and build. They are economically one of the most important extensions of classical filters and have reached operating frequencies of more than 10 GHz.

The surface of a piezoelectric substrate such as monocrystalline barium-titanate or -tantalate carries input and output transducers as shown in Fig. 41. They translate the electrical field E stemming from the input voltage V_1 through the piezo-

Table 5. A List of Impedances Z_1 and Z_2 and the Pertinent $a(\omega)$ for Amplitude Equilization.

Z_1	Z_2	Shape of $a(\omega)$ in Eq. (86)
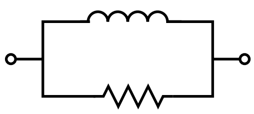	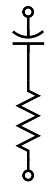	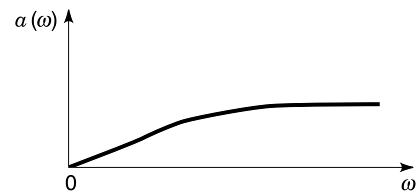
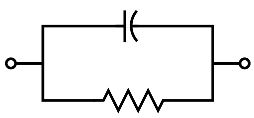	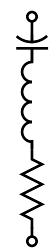	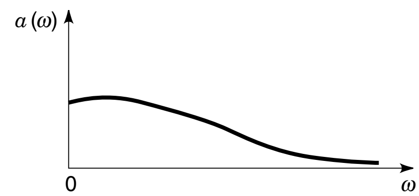
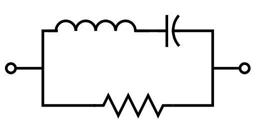	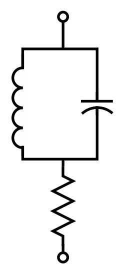	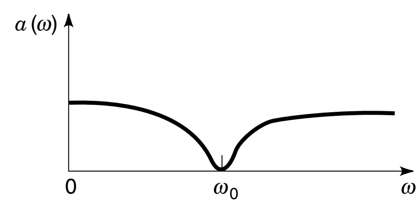
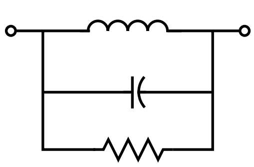	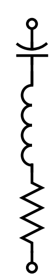	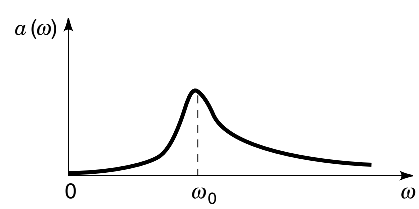

electric effect into a mechanical wave that travels with speed v mainly in the surface of the substrate to the output transducer. Waves traveling backward or through the bulk of the substrate disappear in an absorbing layer in Figs. 41 and 42. The inverse piezo effect changes the mechanical wave in the output transducer back to a charge separation, resulting in the output voltage V_2.

In its simplest form, the fingers and the gaps of the transducers exhibit all the same width as depicted at the top of Fig. 43. In a more complicated but also more versatile case, they are all unequal, as shown also in Fig. 43. The latter layout provides more degrees of freedom for the filter design. The electrical field in the gaps as response to Dirac impulses at the input reaches infinite values in the borders of the fingers, as depicted in Fig. 43. This shape is approximated also by Dirac impulses, as drawn in the last plot in Fig. 43. This so-called δ-approximation renders the calculation of the transfer function $F(p)$ rather easy. Each location of a δ-impulse is the origin of a mechanical δ-impulse traveling with the speed v to the output transducer. Figure 44 shows the distances from the pair of fingers μ in the input transducer to the pair of fingers ν in the output transducer; in Fig. 44 x_0 is the distance between the last fingers of the input transducer and the first fingers of the output transducer. A most important parameter is the overlap h_μ (respectively, g_ν) of a pair of fingers in the transducers. They determine the width of the wave leaving the input and being received by the output. Due to diffraction, the width expands while the wave travels through the sub-

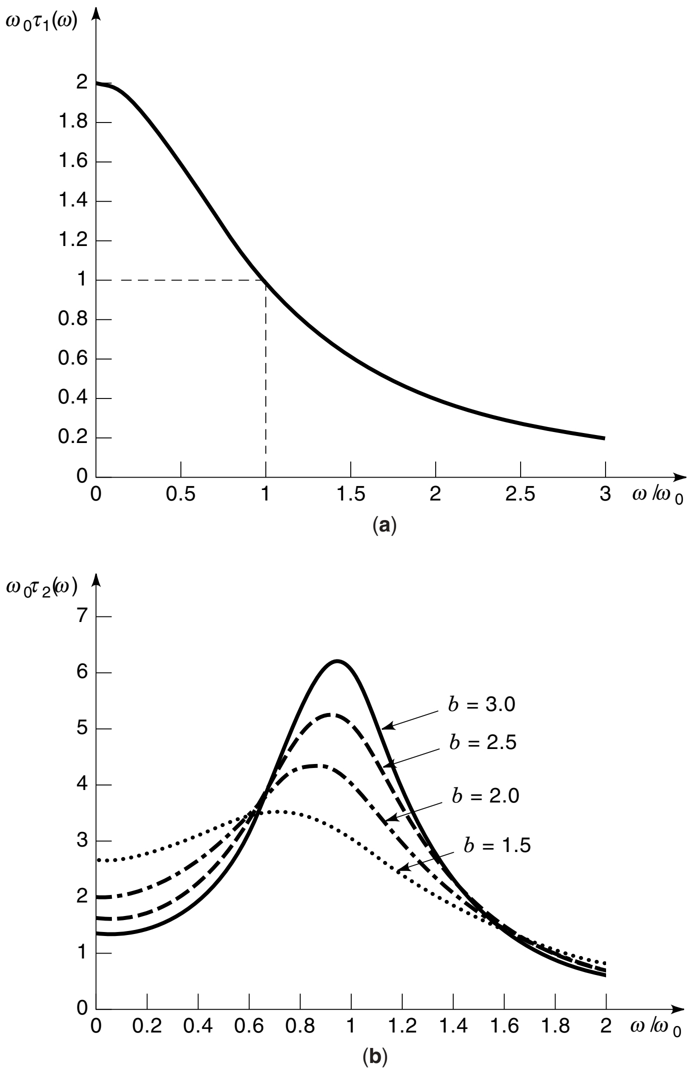

Figure 39. (a) The group delay of a first-order allpass in Eq. (87). (b) The group delay of a second-order allpass in Eq. (88).

strate. This effect is limited by the dummy electrodes in Fig. 41. They form a surface with equal potential from where the wave again starts with a given width.

The two δ-impulses in the edges of the finger pair μ in the input transducer in Fig. 44 reach the center of the gap of the finger pair ν in the output transducer after the delays

$$t_{L_1} = \frac{x_0 + (\nu + \mu)r + q_\mu}{v} \tag{91}$$

and

$$t_{L_2} = \frac{x_0 + (\nu + \mu)r - p_\mu}{v} \tag{92}$$

with

$$p_\mu = c + b_\mu \tag{93a}$$

and

$$q_\mu = c - d_\mu \tag{93b}$$

generating the voltage

$$e_{\mu\nu}(t) = k(\delta(t - t_{L_1}) + \delta(t - t_{L_2})) \tag{94a}$$

with

$$k = \frac{k_0}{p_\mu + q_\mu}(-1)^\nu(-1)^\mu \min(h_\mu, g_\nu) \tag{94b}$$

The factor k describes the strength (area) of the impulse, which is inversely proportional to the width of the gap $1/(p_\mu + q_\mu)$ of finger pair μ, proportional to the $\min(h_\mu, g_\nu)$ because the minimum of either the width h_μ of the transmitted wave or the width g_ν of the overlap of the receiving finger pair determines the received wave, and, finally, proportional to the alternating sign of E in the gaps represented by $(-1)^\nu(-1)^\mu$; k_0 is a factor of proportionality representing the transducer constant. As a synthesis with $\min(h_\nu, g_\mu)$ is hard to achieve, we put

$$\min(h_\nu, g_\mu) = h_\mu \tag{95}$$

meaning $g_\nu > h_\mu$ for all ν and μ; thus the output transducer receives the full energy transmitted by the input transducer.

The full impulse response $h(t)$ of the SAW filter is given by adding over all N transmitting finger pairs and over all M receiving pairs, which provides, with Eqs. (91) through (95),

$$h(t) = \sum_{\mu=0}^{N-1}\sum_{\nu=0}^{M-1} \frac{k_0(-1)^{\nu+\mu}h_\mu}{2c + b_\mu - d_\mu}\left(\delta\left(t - \frac{x_0 + (\nu+\mu)r + c - d_\mu}{v}\right) + \delta\left(t - \frac{x_0 + (\nu+\mu)r - c - b_\mu}{v}\right)\right) \tag{96}$$

A Laplace transform of Eq. (96) yields the transfer function

$$F^*(j\omega) = k_0 e^{j\omega x_0/v}\sum_{\mu=0}^{N-1}\sum_{\nu=0}^{M-1}(-1)^{\nu+\mu}\frac{h_\mu}{2c + b_\mu - d_\mu}\, e^{-j\omega(\nu+\mu)r/v} \left[e^{-j\omega c/v}e^{j\omega d_\mu/v} + e^{j\omega c/v}e^{j\omega b_\mu/v}\right] \tag{97}$$

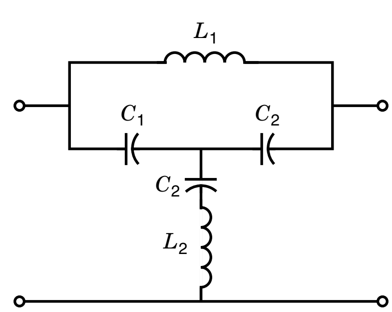

Figure 40. Bridged-T network realizing a second-order allpass with constant input and output impedances R for the element values

$$L_1 = 2\frac{R^2C_1C_2}{2C_1 + C_2} \quad L_2 = \frac{1}{2}R^2C_1$$

and for a termination by R.

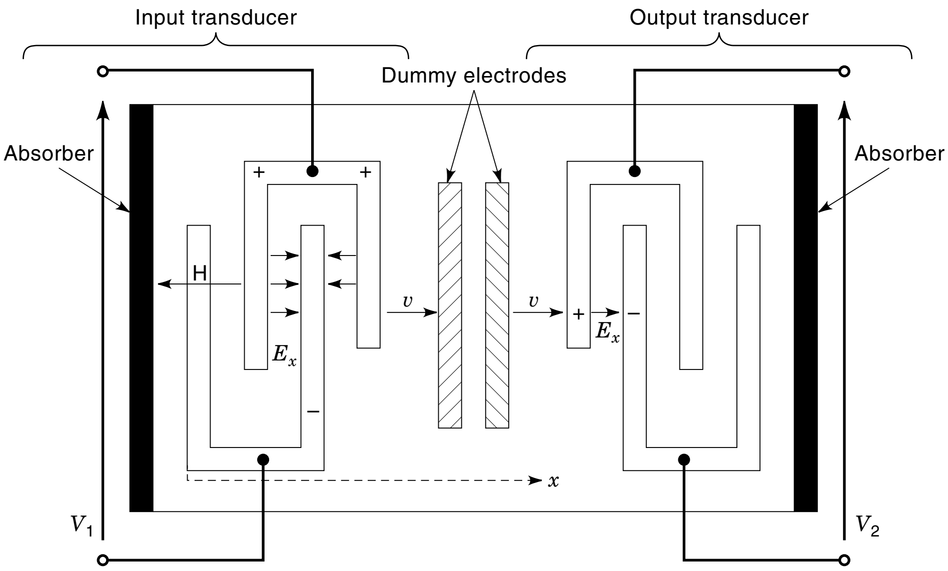

Figure 41. Top view on surface acoustic wave filter (SAW filter).

This general result is, for practical applications, usually simplified by setting $b_\mu = 0$ and $d_\mu = 0$ for all μ, which means that all fingers have the same width $r/2$, which is also the width of all gaps. This reduces $F^*(j\omega)$ in Eq. (97) to

$$F^*(j\omega) = \frac{k_0}{c}\cos\frac{c\omega}{v}\, e^{-j\frac{\omega x_0}{v}} \sum_{\mu=0}^{N-1} (-1)^\mu h_\mu e^{-j\omega\,\mu r/v} \sum_{\nu=0}^{M-1} (-1)^\nu e^{-j\omega\,\nu r/v} \tag{98}$$

In Eq. (98) the term $e^{-j\omega x_0/v}$ stands for the delay x_0/v of the wave between the two transducers; the sum over ν is the essentially unwanted contribution of the output transducer, whereas the cos term stems from the two δ-impulses per finger pair. The desired frequency characteristic has to be realized with the individual overlaps h_μ of the input transducer. We set

$$(-1)^\mu h_\mu = h'_\mu \tag{99a}$$

and

$$z = e^{j\omega r/v} \tag{99b}$$

and obtain from Eq. (98)

$$\frac{F^*(j\omega)}{\dfrac{k_0}{c}\cos\dfrac{c\omega}{v}\, e^{-j\omega x_0/v} \displaystyle\sum_{\nu=0}^{M-1} (-1)^\nu e^{-j\omega\,\nu r/v}} = \sum_{\mu=0}^{N-1} h'_\mu z^{-\mu} \tag{100}$$

$F^*(j\omega)$ is the desired transfer function to be synthesized; the denominator on the left-hand side of Eq. 100 is the unavoidable contribution of the transducers. The ratio of both terms on the left has to be approximated by the right-hand term. This term is the same as the transfer function of digital filters with finite impulse response (FIR filters). Therefore, the synthesis procedures known from FIR filters can be applied (21,22). Even though SAW filters are continuous time systems, the approximation by δ-impulses renders them similar to time discrete systems, where r/v in Eq. (99b) plays the role of the sampling time.

We cannot expect the approximation to provide h'_μ with alternating signs. Hence the layout of the fingers must be modified according to Fig. 45, where the alternation of signs is interrupted.

The pitch r in Fig. 46 is chosen such that the output signal is maximum at the center frequency of the passband. This is achieved by a constructive interference of the wave traveling the distance $2r$ in time $2r/v$ and the sin wave with frequency ω_0 imposed by the voltage V_1 exhibiting the period $2\pi/\omega_0$. This yields

$$\frac{2r}{v} = \frac{2\pi}{\omega_0}$$

or

$$r = \frac{v\pi}{\omega_0} = \frac{v}{2f_0} \tag{101}$$

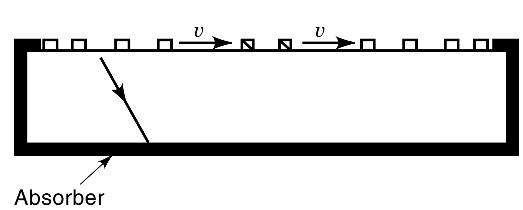

Figure 42. Cross section of SAW filter.

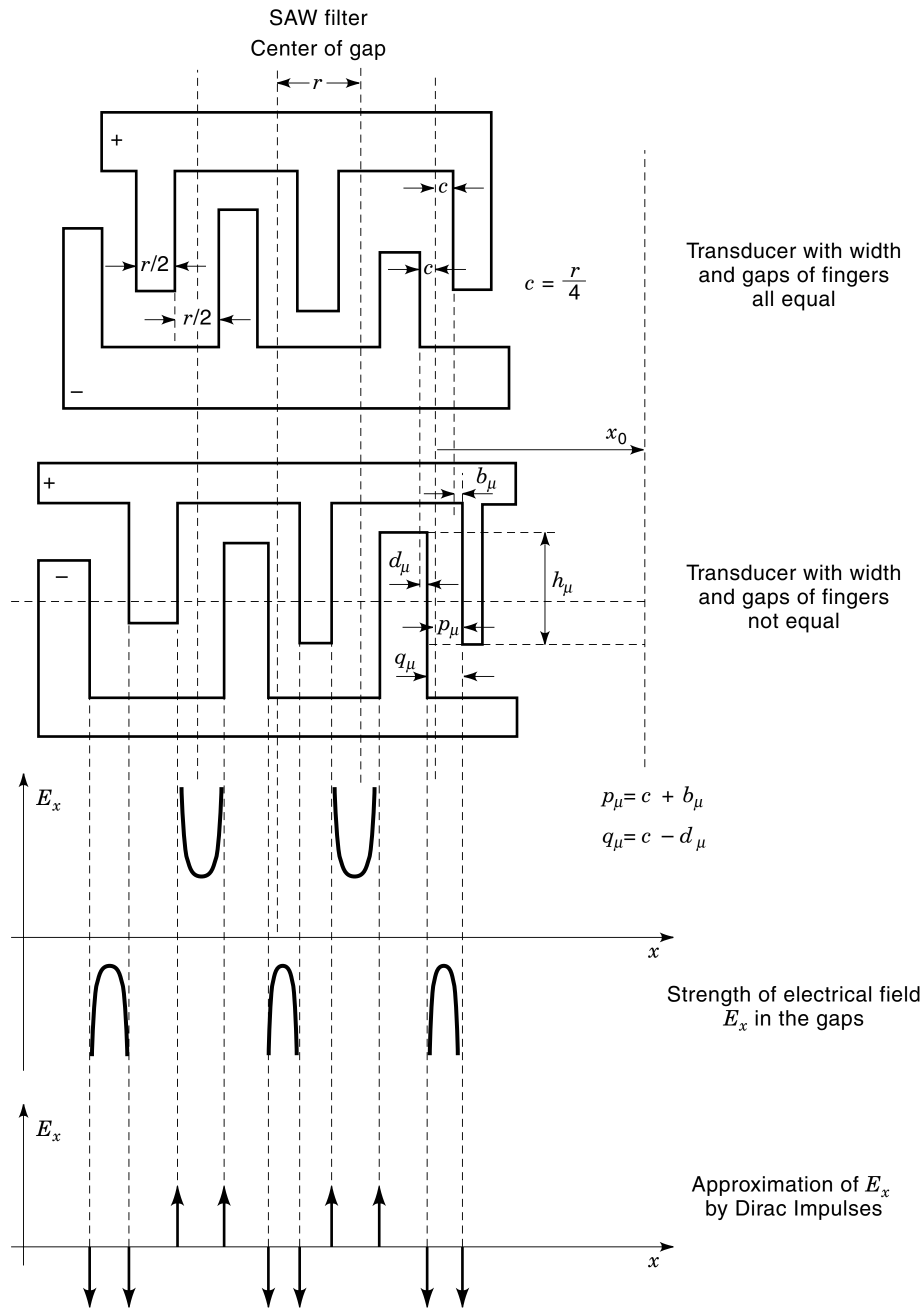

Figure 43. Top view of fingers and electrical field in the gaps.

Due to the approximations made, the design of SAW filters as a rule requires a corrective redesign based on the measured deviations from the desired characteristics. Further damaging parasitic effects are the triple transit signals, which are reflected by the fingers at the output transducer and then again reflected back to the output by the input transducer.

Economically important applications of the SAW technology are filters for the intermediate frequency in TV sets and filters for mobile communications.

The bandpass for TV sets possesses a center frequency of 38 MHz; the SAW substrate exhibits $v = 1000$ m/s. This yields, according to Eq. (101), a width of the fingers that equals the gaps of $r/2 = 13\ \mu$m. A shortcoming of SAW filters is the relatively large insertion loss in the passband of around 8 dB, stemming mainly from the loss in the substrate material. The loss can be decreased to around 5 dB by employing a second output transducer in Fig. 47, which catches the so far unused backward-traveling wave. However, the placement of the two output transducers both in the distance x_0 has to be accurate in order to maintain the same phase of the waves added in the output transducers.

AREAS FOR FUTURE STUDY

Classical filter synthesis is a well-established area for which the first contributions were published more than 70 years ago. Most of the important problems were indeed solved in the meantime. Some remaining unresolved problems will be

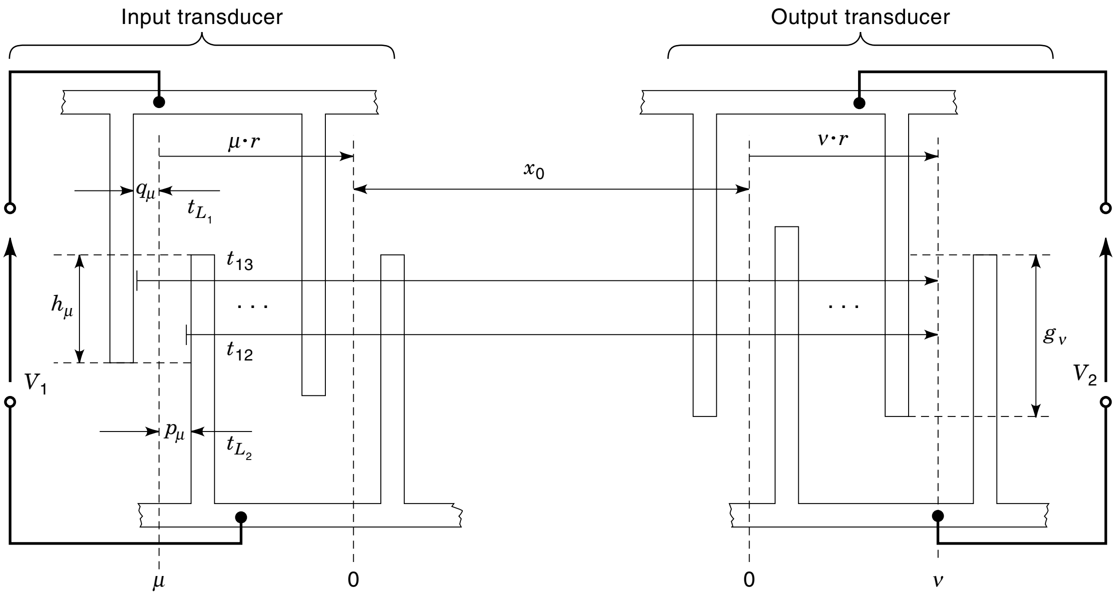

Figure 44. Top view of input and output transducer with unequal widths and gaps of fingers.

outlined in this section. There has been increased focus on those problems in recent years because the classical filters serve as models for filter implementations in new technologies, such as digital filters, *RC*-active filters, and switched-capacitor filters.

The following problems need to be resolved:

1. A proof that the synthesis of lossless two-ports with partial and full pole removal is always possible with realizable reactances is still missing. It is a difficult task, as many unsuccessful attempts may testify. However, a proof would certainly offer a deeper insight into one of the most important synthesis procedures. A helpful hint for further investigations would be the fact that negative impedances are also tolerable for partial pole removal, as they can represent the negative component, an inductor or a capacitor, in the equivalent circuit for a transformer with tight couplings.
2. Guidelines on how to find lossless two-ports with a minimum number of the more expensive inductors would be of economic interest. The guidelines could make use of the large number of equivalent solutions.
3. A procedure is needed to control the various possibilities for synthesizing a lossless two-port such that the component values lie in a desired range. This could help

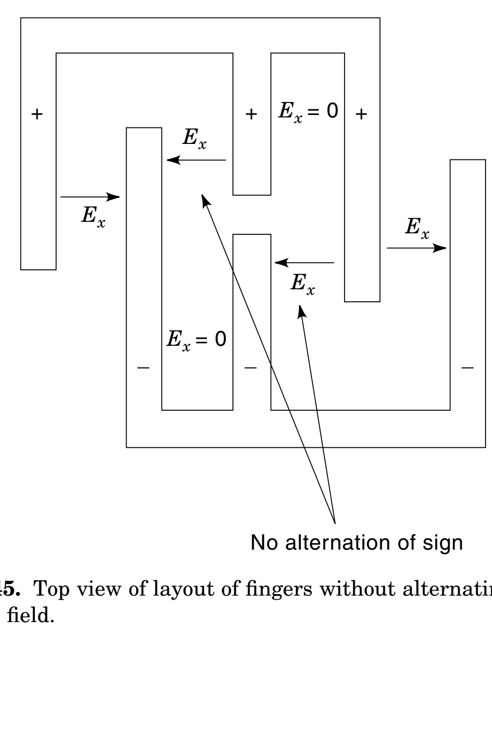

Figure 45. Top view of layout of fingers without alternating signs of electrical field.

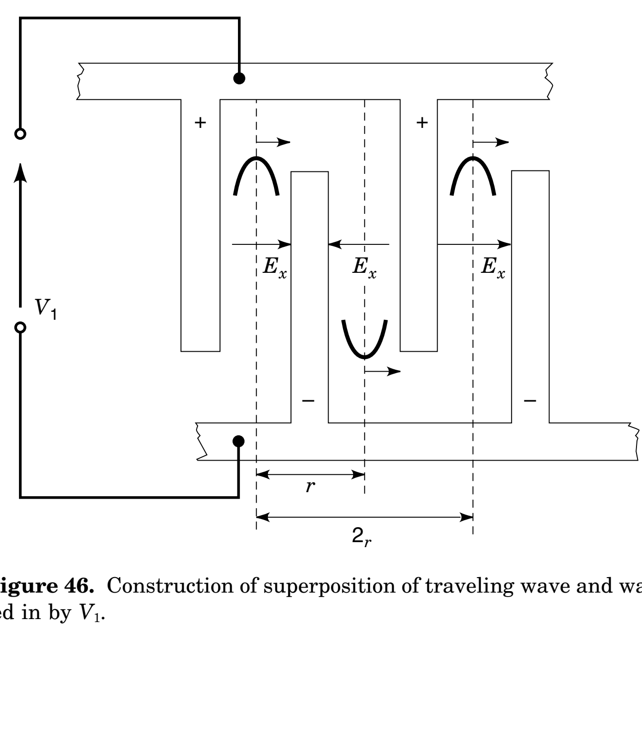

Figure 46. Construction of superposition of traveling wave and wave fed in by V_1.

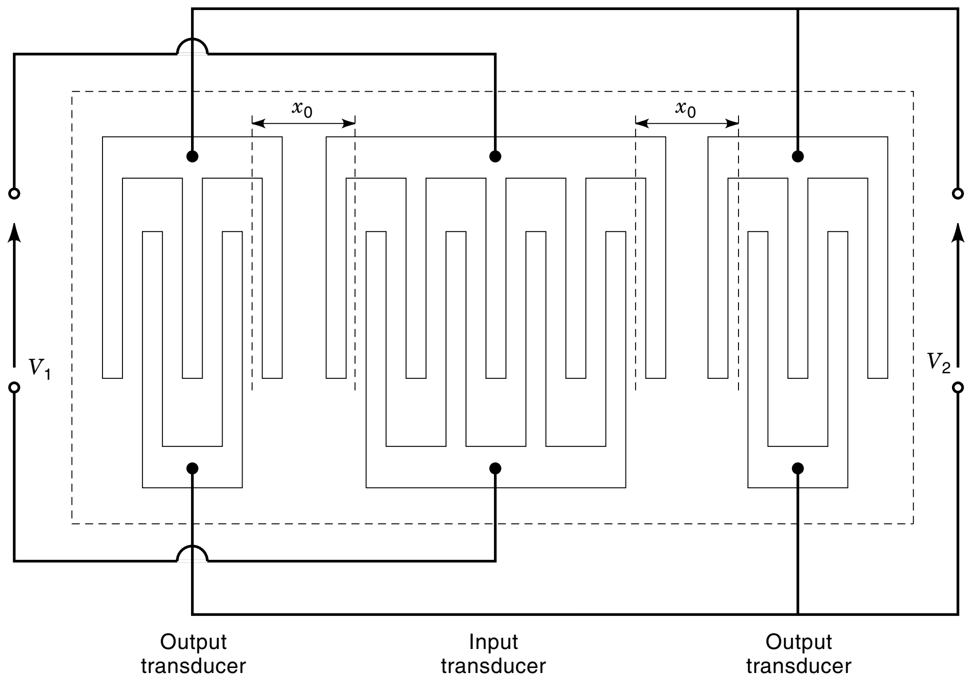

Figure 47. SAW filter with two parallel connected output transducers in two identical distances x_0 from the input transducer.

in using the components of an advantageous price- and performance category and in implementing parasitic components of a given value.

For filters in new miniaturized technologies, the solution to the problem could provide component values that are feasible in the new technology, such as multipliers with values in the raster 2^{ν}, ν integer, in digital signal processing or capacitors in the pF range for CMOS technology while still maintaining a closed-loop gain around 1 of the operational amplifiers. The same goal may be reached by a linear transformation into an equivalent two-port either for the time continuous classical filters (12,23) or for digital filters (24).

4. A method is needed to generate equivalent reactance circuits for nonelectric components, such as coupled quartz oscillators, or for other mechanical oscillators during the synthesis procedure for lossless two-ports.
5. In the approximation method based on a conformal mapping, the approximation of arbitrary but realizable requirements in the stopband by a minimum number of coth $|(\gamma_i - \gamma)/2|$ functions should be achieved by an analytical solution and not by a search procedure, guaranteeing that the minimum number of coth functions is always reached. This design method would be one of the most powerful.
6. There is a need for synthesis of *RLC* two-ports that also include lossy two-ports with a complex impedance as a load and as internal impedance of the voltage source. This becomes more important the higher the operating frequencies are, which imply complex impedance loads. The synthesis of either lossy two-ports with resistive loads or of lossless two-ports with complex impedance loads (25) has been solved. Still unknown is the synthesis of two-ports combining the two properties.
7. There is a need for synthesis of SAW filters based on a more accurate but still easy-to-handle simulation of the device, which should eliminate the need for a corrective redesign.
8. A straightforward synthesis of SAW filters with the large number of geometrical parameters in Eq. (69) will save fingers and hence chip area. The synthesis should also compensate for parasitic effects, such as the triple transit signal.
9. Materials science ought to synthesize piezoelectric substrates with a diminished attenuation of the SAW in order to decrease the insertion loss of filters.

ACKNOWLEDGMENTS

The author acknowledges the valuable discussions with and the proofreading by his coworkers Markus Gaida, Joachim Selinger, Axel Wenzler, Markus Wintermantel, and Christof Zeile.

BIBLIOGRAPHY

1. W. Bader, Elektrische Netzwerke mit vorgeschriebenem Einschwingvorgang, *VDE-Fachberichte,* **13**: 289–295, 1949.
2. E. Lueder, *Die Verwirklichung der Kettenmatrix des allgemeinen passiven Vierpols durch eine Schaltung mit der geringsten Zahl von Teilen,* Habilitationsschrift, University of Stuttgart, 1966.
3. S. Darlington, Synthesis of reactance four-poles which produce prescribed insertion loss characteristics, *J. Math. Phys.,* **18**: 257–353, 1939.
4. R. W. Daniels, *Approximation Methods for Electronic Filter Design,* New York: McGraw-Hill, 1974.
5. M. S. Ghausi, *Principles and Design of Linear Active Circuits,* New York: McGraw-Hill, 1965.
6. D. O. Pederson and E. S. Kuh, *Principles of Circuit Synthesis,* New York: McGraw-Hill, 1959.

7. L. Weinberg, *Network Analysis and Synthesis,* International Student Edition, New York: McGraw-Hill, 1962.
8. S. K. Mitra, *Analysis and Synthesis of Linear Active Networks,* New York: Wiley, 1969.
9. S. Butterworth, On the theory of filter amplifiers, *The Wireless Engineer,* **13**: 536–541, 1930.
10. Private communication by A. Wenzler and M. Wintermantel, Institute of Network and Systems Theory, University of Stuttgart, 1997.
11. W. E. Thomson, Delay networks having maximally flat frequency characteristics, *Proc. IEEE, part 3,* **96**: 487–490, 1949.
12. W. Cauer, *Synthesis of Linear Communication Networks,* transl. from the German by G. E. Knausenberger, 2nd. ed., New York: McGraw-Hill, 1958.
13. R. Saal and W. Entenmann, *Handbuch zum Filterentwurf* [*Handbook of Filter Design*], 2nd ed., Heidelberg: Hüthig, 1988.
14. E. Christian and E. Eisenmann, *Filter Design Tables and Graphs,* New York: Wiley, 1966.
15. R. Saal, *Der Entwurf von Filtern mit Hilfe des Kataloges normierter Tiefpässe,* Backnang: Allg. Electricitäts-Ges. AEG-Telefunken, 1968.
16a. W. Bader, Kopplungsfreie Kettenschaltungen, *Telegraphen-Fernsprech-Funk- und Fernseh-Technik,* **31**: 177–189, 1942.
16b. W. Bader, Kettenschaltungen mit vorgeschriebener Kettenmatrix, *Telegraphen-Fernsprech-Funk- und Fernseh-Technik,* **32**: 119–125, 144–147, 1943.
16c. W. Bader, Polynomvierpole vorgeschriebener Frequenzabhängigkeit, *Archiv Für Elektrotechnik,* **34**: 181–209, 1940.
17. H. Piloty, Über die Realisierbarkeitssätze der Kettenmatrix von Reaktanzvierpolen, *Telegraphen-Fernsprech-Funk- und Fernseh-Technik,* **30**: 217–223, August 1941.
18. R. M. Foster, A reactance theorem, *Bell Syst. Tech. J.,* **3**: 259–267, 1924.
19. E. Guillemin and S. A. Ernst, *Synthesis of Passive Networks: Theory and Methods Appropriate to the Realization and Approximation Problems,* New York: Wiley, 1957.
20. M. E. Van Valkenburg, *Analog Filter Design,* New York: Holt, Rinehart & Winston, 1982.
21. B. Gold and C. M. Rader, *Digital Processing of Signals,* New York: McGraw-Hill, 1969.
22. S. K. Mitra and J. F. Kaiser, *Handbook for Digital Signal Processing,* New York: Wiley, 1993.
23. E. Lueder, *Äquivalente Schaltungen und Topologie der Schaltungen geringsten Aufwandes,* Ph.D. Thesis, University of Stuttgart, June 1962.
24. E. Lueder and K. Haug, Calculations of all equivalent and canonic 2nd order digital filter structures, *IEEE Int. Conf. Acoustics, Speech Signal Process,* Tulsa, April 10–12, 1978, pp. 51–54.
25. W. Bader, Die Synthese des linearen passiven Vierpoles bei beliebigen komplexwertigen Quellen- und Abschlußwiderständen, *Nachrichtentechnische Zeitschrift,* 549–555, November 1964.

Reading List

L. O. Chua, C. A. Desoer, and E. S. Kuh, *Linear and Non-Linear Circuits,* New York: McGraw-Hill, 1997.

ERNST LUEDER
University of Stuttgart

FILTERS, TIME-VARYING. See TIME-VARYING FILTERS.